CLEPS: A new protocol for cloud aqueous phase oxidation of VOC mechanisms

Camille Mouchel-Vallon[1,2,a], Laurent Deguillaume[1,2], Anne Monod[3], Hélène Perroux[1,2], Clémence Rose[1,2], Giovanni Ghigo[4], Yoann Long[1,2,b], Maud Leriche[5,6], Bernard Aumont[7], Luc Patryl[8], Patrick Armand[8], Nadine Chaumerliac[1,2]

[1]Université Clermont Auvergne, Université Blaise Pascal, OPGC, Laboratoire de Météorologie Physique, BP 10448, 63000 Clermont-Ferrand, France
[2]CNRS, LaMP/OPGC, UMR6016, BP80026, 63177 Aubière, France
[3]Aix Marseille Université, CNRS, LCE UMR 7376, 13331, Marseille, France
[4]Dipartimento di Chimica, Universita di Torino, V. Giuria 7, I-10125 Torino, Italy
[5]Université de Toulouse, UPS, Laboratoire d'Aérologie, 14 avenue Edouard Belin, 31400 Toulouse, France
[6]CNRS, LA, UMR 5560, 31400 Toulouse, France
[7]LISA UMR CNRS 7583, Université Paris Est Créteil et Université Paris Diderot, Paris, France
[8]CEA, DAM, DIF, F-91297 Arpajon, France
[a]Now at: Wolfson Atmospheric Chemistry Laboratories, Department of Chemistry, University of York, Heslington, York, YO10 5DD, United Kingdom
[b]Now at: Ramboll Environ, 155 rue Louis de Broglie, 13100 Aix-en-Provence, France

Correspondence to: L. Deguillaume (l.deguillaume@opgc.univ-bpclermont.fr), C. Mouchel-Vallon (camille.mouchel-vallon@york.ac.uk)

Abstract. Organic compounds of both anthropogenic and natural origin are ubiquitous in the multiphasic atmospheric medium. Their transformation in the atmosphere affects air quality and the global climate. Modelling provides a useful tool to investigate the chemistry of organic compounds in the tropospheric multiphase system. While several comprehensive explicit mechanisms exist in the gas phase, explicit mechanisms are much more limited in the aqueous phase.

Recently, new empirical methods have been developed to estimate HO$^•$ reaction rates in the aqueous phase: structure-activity relationships (SARs) provide global rate constants and branching ratios for HO$^•$ abstraction from and addition to atmospheric organic compounds. Based on these SARs, a new detailed aqueous-phase mechanism, named the cloud explicit physico-chemical scheme (CLEPS), to describe the oxidation of hydrosoluble organic compounds resulting from isoprene oxidation is proposed. In this paper, a protocol based on reviewed experimental data and evaluated prediction methods is described in detail. The current version of the mechanism includes approximately 850 aqueous reactions and 465 equilibria. Inorganic reactivity is described for 67 chemical species (*e.g.*, transition metal ions, H_xO_y, sulphur species, nitrogen species, and chlorine). For organic compounds, 87 chemical species are considered in the mechanism, corresponding to 657 chemical forms that are individually followed (*e.g.*, hydrated forms, anionic forms). This new aqueous-phase mechanism is coupled with the detailed gas phase mechanism MCM v3.3.1 through mass transfer parameterization for the exchange between the gas phase and aqueous phase. The GROMHE SAR enables the evaluation of the Henry's law constants for undocumented organic compounds. The resulting multiphase mechanism is implemented in a model based on the Dynamically Simple Model for Atmospheric Chemical Complexity (DSMACC) using the Kinetic PreProcessor (KPP). This model allows simulation of the time evolution of the concentrations of each individual chemical species in addition to detailed time-resolved flux analyses. The variable photolysis in both phases is calculated using the TUV 4.5 radiative transfer model.

To evaluate our chemical mechanism, an idealized cloud event with fixed microphysical cloud parameters is simulated. The simulation is performed for a low-NO$_x$ situation. The results indicate the formation of oxidized mono- and diacids in the aqueous phase, as well as a significant influence on the gas phase chemistry and composition. For this particular simulation, the aqueous phase mechanism is responsible for the efficient fragmentation and functionalization of organic compounds. This new cloud chemistry model allows for the analysis of individual aqueous sub systems and can be used to analyze the results from cloud chamber experiments and field campaigns.

1 Introduction

Clouds favour chemical reactions that would not occur in the gas phase or at a rate much slower than in the aqueous phase (Epstein and Nizkorodov, 2012; Herrmann, 2003; Herrmann et al., 2015). Reactivity in clouds is due to (1) highly enhanced photochemical processes in cloud droplets; (2) faster aqueous phase reactions than in clear sky, some of which do not occur

5   in the gas phase, especially those involving ions and hydration; (3) possible interactions between the aqueous phase and particulate phase. Clouds can also be responsible for secondary organic aerosol (SOA) formation and ageing. However, aqueous phase processes suffer from large uncertainties. Blando and Turpin (2000) first proposed clouds as a source of SOAs. Recent field measurements (Kaul et al., 2011; Lee et al., 2012, 2011), experimental work (Brégonzio-Rozier et al., 2016) and modelling studies (Ervens, 2015; Ervens et al., 2011) have shown that aqueous phase processes could lead to SOA

10 formation on the same order of magnitude as gas phase processes. The contribution of cloud and fog processes to SOA formation is firstly indirect, through the effects of cloud chemistry on the oxidant budget. Gas phase reactivity of volatile organic compounds (VOC) is controlled by daytime HO$^\bullet$ oxidation, and it has been shown that radical chemistry in the aqueous phase plays a significant role in the budget of this oxidant (Herrmann et al., 2015). Secondly, cloud and fog processes act directly on SOA sinks and sources. Dissolution and processing of organic vapour in the aqueous phase can lead

15 to the formation and destruction of SOA precursors through accretion (*i.e.,* carbon-carbon bond formation) and oxidation processes. These processes may compete in the aqueous phase (Kirkland et al., 2013; Renard et al., 2015), simultaneously acting as the source (through oligomerization and functionalization reactions) and sink (through fragmentation reactions) of SOAs. To elucidate the contribution of accretion and oxidation to the budget of SOA precursors, most recent studies on the topic have focused on the modelling and measuring of accretion processes (Ervens et al., 2015). However, equivalent

20 knowledge of aqueous oxidation is needed because oxidation processes may control the availability of organic compounds and radicals to form accretion products. In this work, we therefore focus on aqueous oxidation processes, especially the competition between fragmentation and functionalization.

Competition between fragmentation and functionalization processes has been identified as a major factor in the production of SOA in the gas phase (Donahue et al., 2012; Jimenez et al., 2009). To better represent these processes in clouds, detailed

25 multiphase mechanisms are needed. Such mechanisms are available for gas phase chemistry (Aumont et al., 2005; Jenkin et al., 1997), whereas very few exist for the aqueous phase. Among the aqueous phase mechanisms, the most cited is Chemical Aqueous Phase Radical Mechanism version 3.0 (CAPRAM 3.0). CAPRAM 3.0 represents one oxidation pathway for each considered species (Herrmann et al., 2005; Tilgner and Herrmann, 2010; Whalley et al., 2015), even if simple organic molecules react at several distinct oxidation sites at comparable rates. As a consequence, there is a loss of information in

30 such mechanism that does not accurately represent both fragmentation and functionalization. To fill this gap, a new protocol is proposed to create an explicit aqueous phase oxidation mechanism to accurately represent the various oxidation pathways of organic matter: the Cloud Explicit Physicochemical Scheme (CLEPS).

This protocol is developed under low-NO$_x$ and dilute conditions and uses recently available laboratory data and empirical estimation methods. This mechanism is implemented in a box model including the gas phase chemistry and kinetic mass

35 transfer of soluble species between the gas phase and cloud droplets. The box model is tested in an ideal cloud situation.

2 Overview

The aqueous phase oxidation mechanism originally relied on inorganic chemistry (see Deguillaume et al., 2004; Leriche et al., 2007) and the oxidation of several organic C$_1$ and C$_2$ species, including photooxidation of iron complexes with oxalic acid (Long et al., 2013). The inorganic processes taken into account in CLEPS are described in Deguillaume et al. (2004)

40 and Long et al. (2013). This inorganic mechanism simulates the redox processes involved in the evolution of H$_x$O$_y$, sulphur, nitrogen, halogen (Leriche et al., 2000, 2003) and transition metal ions (TMIs; Deguillaume et al., 2004). A special emphasis

is given to the latter, as the speciation of TMIs is believed to drive the evolution of aqueous phase oxidants (H_2O_2, $HO^\bullet$, $HO_2^\bullet/O_2^{\bullet-}$; Deguillaume et al., 2005) (see R14 to R95 in the mechanism tables). In the present study, the CLEPS mechanism is extended to the oxidation of C_{1-4} precursors and follows the protocol described in detail in sections 3 and 4. Although isoprene is not significantly dissolved in the atmospheric aqueous phase, its oxidation products are considered. For instance

5   methylglyoxal (MGLY), glyoxal (GLY), acrolein (ACR), methacrolein (MACR) and methylvinylketone (MVK) are significantly soluble and highly reactive in the aqueous phase (Ervens and Volkamer, 2010; Lim et al., 2010, 2013; Liu et al., 2009, 2012).

For each species and its oxidation products, the CLEPS mechanism describes the oxidation of $HO^\bullet$ (section 3.3) and $NO_3^\bullet$ (section 3.4) and the explicit evolution of the produced peroxyl radicals (section 4). When data are available, the reactivity of

10   organic compounds with other oxidants ($SO_4^\bullet$, $Cl_2^\bullet$,…) is also addressed (section 3.5). Hydration (section 3.1) and dissociation (section 3.2) equilibria are, respectively, considered for carbonyl and carboxylic functions.

Moreover, recent developments in empirical estimates of kinetic and thermodynamic parameters (*e.g.*, reaction rates, Henry's law constants) for aqueous phase chemistry (Doussin and Monod, 2013; Minakata et al., 2009; Monod and Doussin, 2008; Raventos-Duran et al., 2010) are included in the CLEPS mechanism. These structure activity relationships (SARs) are

15   based on experimental data and rely on robust hypotheses about the reaction rates (section 3.3.2) and equilibrium constants (sections 3.1 and 3.2) of species that are not documented in the literature. For instance, SARs can provide estimations of the branching ratios between the different oxidation pathways with $HO^\bullet$ radicals (Doussin and Monod, 2013; Minakata et al., 2009; section 3.3.3).

The mechanism currently includes 850 aqueous reactions and 465 equilibria. Inorganic reactivity is described for 67

20   chemical species (*e.g.*, TMIs, H_xO_y, sulphur species, nitrogen species and chlorine). For organic compounds, 87 chemical species are considered in the mechanism corresponding to 657 chemical forms (*e.g.*, hydrated forms, anionic forms).

3 Stable organic species

3.1 Hydration equilibria

Carbonyls, *i.e.,* aldehydes and less likely ketones, may undergo hydration leading to the formation of a gem-diol form:

25   **R.1** $>CO + H_2O \overset{K_{hyd}}{\longleftrightarrow} >C(OH)(OH)$
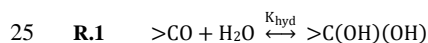
K_{hyd} [dimensionless] is the hydration constant and is defined as:

Eq.1 $K_{hyd} = \dfrac{>C(OH)(OH)}{>CO}$

There are 30 carbonyl species in the mechanism. Most of the C_{1-2} species are well known and data are available in the literature. However, there is a lack of data for C_{3-4} species, and empirical estimates must be performed.

30   To the best of our knowledge, there is only one SAR available to estimate hydration constants (Raventos-Duran et al., 2010); it is provided by the GROMHE SAR for Henry's law constants. This SAR is based on five descriptors and is optimized on a dataset comprising 61 species. Raventos-Duran et al. (2010) defined a global descriptor, *tdescriptor*, to represent functional group interactions with the sum of the so-called sigma Taft values (σ^*, *e.g.,* Perrin et al., 1981). Similarly, *hdescriptor* is a global descriptor representing the inductive effect of functional groups attached to an aromatic ring through the sum of the

35   meta-, para- and ortho-Hammett sigma values (σ_m, σ_p and σ_o, respectively; *e.g.,* Perrin et al., 1981; for more details see Raventos-Duran et al., 2010). It is applied for all stable carbonyl species when a measured value is not available. However, this method was originally developed only for stable non-ionic species.

In the present study, the SAR is extended to anionic species. The descriptors have been optimized to include the Taft and Hammett sigma values for the carboxylate moieties ($\sigma^*(-CO(O^-)) = -1.06$, $\sigma_m(-CO(O^-)) = 0.09$, $\sigma_p(-CO(O^-)) = -0.05$ and $\sigma_o(-$

CO(O⁻)) = -0.91; Perrin et al., 1981). The database from Raventos-Duran et al. (2010) has been extended to carboxylate species with measured values available in the literature (**Table 1**). Following the same method as Raventos-Duran et al. (2010), multiple linear regression optimization is performed by minimizing the sum of squared errors (SSE):

Eq.2 $\quad SSE = \sum_{i=1}^{n}\left(\log K_{\text{hyd,est}} - \log K_{\text{hyd,exp}}\right)^2$

where n is the number of experimental values in the database (n=65), including both the values compiled and taken into account by Raventos-Duran et al. (2010) and the new carboxylate values. **Figure 1** shows both the previous and the updated values of the descriptors and the performance of the SAR. The new optimization for carboxylate compounds modifies the descriptors by at most 50% for the intercept. The other descriptors vary from 1% (*hdescriptor*) to 18% (*ketone flag*) of their initial values. There is greater uncertainty associated with this new optimization; the root mean square error (RMSE =

$\sqrt{\frac{1}{n}\sum_{i=1}^{n}\left(\log K_{\text{hyd,est}} - \log K_{\text{hyd,exp}}\right)^2}$) is 0.61 log units, which is higher than the RMSE = 0.47 log units given in Raventos-Duran et al. (2010). However, the new optimization is still able to estimate K_{hyd} within a factor of 4 (3 in Raventos-Duran et al., 2010).

Hydration data are not available in the literature for the peroxyl ($RO_2^•$) and acylperoxyl ($RC(=O)(O_2^•)$) radicals. However, there is no reason to ignore the hydration of these radicals. As a first approach, when data are not available, we assign to a given $RO_2^•$ the hydration constant of its parent species. For example, for the radicals derived from glycolaldehyde, we have:

Eq.3 $\quad K_{\text{hyd}}\left(CH_2(OH)CO(OO·)\right) = K_{\text{hyd}}(CH(OH)(OO·)CHO) = K_{\text{hyd}}(CH_2(OH)CHO) = 10$

The lack of experimental data does not allow validation of this hypothesis and excludes further extension of the Raventos-Duran et al. (2010) SAR. This approximation is likely valid when there is no or weak interactions between the peroxyl and carbonyl functions, *i.e.,* when these functions are separated by several carbon atoms. This is also applied to short-chain hydrocarbons and acylperoxyl radicals since it is the only way to counteract the lack of experimental data. When new data become available, they can be easily implemented to replace our hypothesis.

3.2 Acid dissociation equilibria

To represent acid dissociation, the acidity constant K_A [dimensionless] is needed:
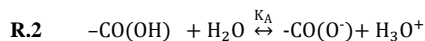
R.2 $\quad -CO(OH) \ + H_2O \overset{K_A}{\leftrightarrow} -CO(O^-) + H_3O^+$

The acidity constant K_A is defined by:

Eq.4 $\quad K_A = \frac{[-CO(O^-)][H_3O^+]}{[-CO(OH)][H_2O]}$

In general, the K_A values are well documented for short-chain organic compounds (C_{1-2}). In the mechanism, each stable acid with one or two carbon atoms can be documented using acidity constant from the literature. This is not the case for C_3 and C_4 species, especially multifunctional species. In the whole mechanism, there are 38 organic acids, 7 of which have a documented K_A value (see Equilibria Tables in the mechanism tables). Like the hydration constants, the acidity constants must therefore be empirically estimated. To obtain the estimates, we use a similarity criterion: if there are no data available in the literature for a given species, the acidity constant from the closest documented species with the same organic function in the α position from the carboxylic acid function is chosen. For example, the acidity constant for pyruvic acid (Lide and Frederikse, 1995) is attributed to 3-oxopyruvic acid because they both carry a ketone function next to the carboxylic acid function, *i.e.*:

Eq.5 $\quad K_A(CHOC(=O)CO(OH)) = K_A(CH_3C(=O)CO(OH) = 10^{-2.4}$
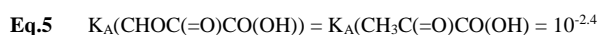
Perrin et al. (1981) showed that the pK_A values of aliphatic organic species are mostly influenced by the inductive effect of the organic function closest to the acidic function. Therefore, this first hypothesis should provide a good estimation of undetermined acidity constants.

Following the hydration constant treatment, the acidity constants for peroxyl radicals are initially taken from their parent species when experimental data are not documented. This assumption can be questioned but very few measurements suggest that peroxyl radicals are more acidic than their parent species. Schuchmann et al. (1989) showed that the acetic acid peroxyl radical ($CH_2(OO^\bullet)CO(OH)$) has a pKa = 2.10, whereas acetic acid has a pKa = 4.76, and they observed the same trend for the malonic acid peroxyl radical, which has a second pKa close to 3 compared to the malonic acid second pKa = 5.7. Therefore, the hydration constants from Schuchmann et al. (1989) are used in the mechanism, and the estimated hydration constants can be directly substituted by laboratory data when the data become available.

3.3 Reaction with HO•

3.3.1 Mechanism

For aliphatic organic compounds, HO• reactivity proceeds by H-abstraction, yielding an alkyl radical following what can occur in the gas phase (Herrmann et al., 2010, 2015):

R.3 $RH + HO\cdot \rightarrow R\cdot + H_2O$

If the compound bears a C=C double bond, the addition is favoured:

R.4 $>C=C< + HO\cdot \rightarrow >C(OH)-C\cdot<$
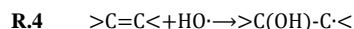
In addition to the gas phase like pathways described above, it may be possible for HO• to undergo electron transfer in the presence of anions, especially carboxylate compounds (von Sonntag and Schuchmann, 1997):

R.5 $-CO\left(O^-\right) + HO\cdot \rightarrow -CO(O\cdot) + OH^-$
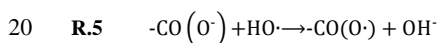
3.3.2 Rates constants

Based on the recent measurements of HO• rate constants for organic compounds reviewed in Herrmann et al. (2010), global reaction rate constants with HO• are used. In the CLEPS mechanism, for a total of 343 reactions with HO•, only 43 kinetic constants are available in the literature. Empirical estimates are thus required in most cases. The estimates are obtained using the recent developments of SARs for the HO• rate. Doussin and Monod (2013) described the extension of a SAR previously published in Monod and Doussin (2008) and Monod et al. (2005). This SAR provides a way to estimate the H-abstraction rate constants for dissolved linear or cyclic alkanes, alcohols, carbonyls, carboxylic acids and carboxylates. This method includes descriptors that consider the effect of functional groups in the α- and β-positions of the abstracted hydrogen atom. For each considered organic moiety, Doussin and Monod (2013) optimized the α- and β-substitution factors. All estimates in the frame of the CLEPS mechanism are within the domain of validity of the Doussin and Monod (2013) SAR.

In the present study, the SAR was modified to account for the electron transfer on carboxylate compounds (R.5). The relevance of this process was discussed by Doussin and Monod (2013). They found an electron transfer rate constant for α-carbonyl carboxylate anions of $k(-C(=O)CO(O^-)) = 2.1\times10^8$ M^{-1} s^{-1}, but it was not included in the original SAR due to the limited amount of experimental data. Their analysis was restricted to the α-carbonyl bases (especially pyruvate and ketomalonate ions, for which electron transfer is dominant), due to the lack of abstractable H-atoms. However, other carboxylate ions could undergo this type of reaction, even if electron transfer is of minor importance because of the faster H-abstraction reactions. Therefore, in the present study, the SAR from Doussin and Monod (2013) has been modified to

include the partial rate constant k(-CO(O⁻)) = 2.1×10^8 M⁻¹ s⁻¹ for each possible electron transfer reaction. This partial rate constant is affected by the α- and β-substitution factors in the same way as the original abstraction constants.

For all unsaturated species in the mechanism (*i.e.,* methylvinylketone - MVK, methacrolein - MACR, hydroxyl-methylvinylketone - MVKOH and hydroxyl-methacrolein - MACROH), the addition reactions rates have been evaluated following the literature and similarity criteria. For further developments involving unknown unsaturated compounds, the SAR from Minakata et al. (2009) should be used because it is the only method that can estimate partial addition rate constants on double bonds.

3.3.3 Branching ratios

Branching ratios are required to identify the most probable oxidation products. In previous mechanisms, the most labile H-atom was empirically identified (*e.g.*, using Bond Dissociation Energy estimations), and the reaction was assumed to proceed exclusively *via* this H-abstraction pathway (Ervens et al., 2003; Tilgner and Herrmann, 2010). This was the only hypothesis that could be considered because experimental data on the branching ratios in aqueous phase HO˙ reactions are extremely scarce. The recent introduction of group-contribution-based SAR (Doussin and Monod, 2013; Minakata et al., 2009) allows estimation of the contribution of each pathway to the global reactivity of each species. In our mechanism, for a given species the global reactivity rate is either provided by the literature or by SAR, but the branching ratios are always obtained from SAR estimates.

Furthermore, for simplicity, a reduction hypothesis was considered in the mechanism for each stable species because explicitly writing all possible reactions would yield a huge number of chemical species. For example, Aumont et al. (2005) showed that the number of species formed in the gas phase for such explicit schemes increases exponentially with the size of the carbon skeleton of the parent species. One can assume based on Aumont et al. (2005) that starting from a C_4 precursor in the aqueous phase, the mechanism would require approximately 10^3 distinct species involved in approximately 10^4 reactions. Such a large of species excludes the development of an aqueous phase oxidation mechanism by hand.

A simple reduction scheme was therefore applied to mitigate this problem and an example is shown in **Table 2** for three selected species. Doussin and Monod (2013) SAR was applied to estimate the contribution of each possible pathway and to maintain at least 75% of the total reactivity. After the reduction is applied, the branching ratios are recalculated to maintain the global oxidation rate constant.

This empirical reduction scheme helps to limit the number of species and reactions (657 different chemical forms representing 87 species reacting in 673 oxidation reactions). This new aqueous phase mechanism then allows consideration of the most probable H-abstraction reaction. For example, in **Table 2** for the hydrated glycolaldehyde, the final reactivity in our mechanism is equally distributed between three HO˙ attack sites and yields 33% glyoxylic acid, 28% glyoxal, 39% formic acid and formaldehyde. This result can be compared with the mechanism of Ervens et al. (2004), which leads to 100% glyoxylic acid since it only considers the abstraction of the aldehydic hydrogen.

Table 2 shows that the Doussin and Monod (2013) SAR estimates often lead to a significant abstraction of the hydrogen atom bonded to the oxygen atom in the hydroxyl moiety. This mechanism has never been addressed in an atmospheric chemical scheme. This reactivity of the alcohol function towards the HO· radical has been experimentally demonstrated by Asmus et al. (1973) for methanol, ethanol, tert-butanol and polyols. To determine whether this reactivity could be extended to all the considered alcohol functions in our mechanism, we investigated whether the process appears thermodynamically feasible by calculating the relative reaction free energies (Gibbs energies) using the Density Functional Theory (DFT, see details and references in the Supplementary Material **SM1**). The thermodynamic values for the reaction enthalpies and Gibbs energies are calculated for the H-abstraction by the HO˙ radical from C and O atoms in the following molecules:

acetaldehyde, propionaldehyde, glycolaldehyde, glyoxal, methylglyoxal, L-lactic acid and L-lactate. H-abstraction from hydrated aldehydes is also included in this study. The results (see Supplementary Material **SM2**) show that H-abstraction is thermodynamically favourable: the reaction enthalpies range from -14 to -47 kcal mol^{-1} and the corresponding free energies range from -13 to -47 kcal mol^{-1}.

3.4 Reaction with NO$_3^\bullet$

NO$_3^\bullet$ is the main night-time oxidant in the gas phase. Although it plays a minor role under low-NO$_x$ conditions, NO$_3^\bullet$ chemistry has been taken into account in the protocol to make it versatile in the future. Previous modelling studies of aqueous-phase reactivity expect the same characteristics for dissolved NO$_3^\bullet$ radicals (Tilgner et al., 2010). For this reason, we represent NO$_3^\bullet$ oxidation for each stable species in the mechanism.

3.4.1 Mechanisms

The mechanism of NO$_3^\bullet$ oxidation is similar to that of HO$^\bullet$ oxidation: the reactivity mainly proceeds via H-abstraction of a labile hydrogen atom to form an alkyl radical and nitric acid:

R.6 $RH + NO_3\cdot \longrightarrow R\cdot + HNO_3$

In this version of the mechanism, the addition of an NO$_3^\bullet$ radical to the C=C double bond is not considered since insufficient data are available for these reactions and for the fate of the resulting organonitrate peroxyl radicals. However, organonitrate compounds were recently identified in the ambient aerosol (Garnes and Allen, 2002; Lee et al., 2016; Rollins et al., 2012). In addition to local emission sources, organonitrate compounds originate from the gas phase chemistry of VOCs under high NO$_x$ conditions (Darer et al., 2011; Farmer et al., 2010; Heald et al., 2010; Paulot et al., 2009; Perring et al., 2013) followed by phase transfer and aqueous processing to the deliquescent aerosol and cloud aerosol phase (Nguyen et al., 2011) to form nitrates, alcohols or organosulphates, which contribute to SOA. In this study, we restricted the simulations to low-NO$_x$ conditions to reduce the potential importance of organonitrate chemistry, which requires further experimental and modelling developments.

3.4.2 Reaction rates

Data concerning NO$_3^\bullet$ reactions rates are available in the literature, mostly for C$_1$ and C$_2$ species (Exner et al., 1994; Gaillard de Sémainville et al., 2007, 2010; Herrmann et al., 2010, 2015). Again, empirical estimates are required to describe the oxidation by NO$_3^\bullet$ radicals when the data are unavailable.

For most C$_{2-4}$ species, we estimate the NO$_3^\bullet$ reaction rates using the similarity criteria. When an estimate is needed, we use the reaction rate of a similar documented species. The primary focus is on the nature, number, and relative position of the organic functions. For example, the reaction rate of 3-hydroxypropionic acid with NO$_3^\bullet$ is estimated to be the same as the reaction rate of lactic acid because both are C$_3$ species with a carboxylic acid and a hydroxyl function:

Eq.6 $k(CH_2(OH)CH_2CO(OH) + NO_3\cdot) = k(CH_3CH(OH)CO(OH) + NO_3\cdot) = 2.1 \times 10^6 \ M^{-1}s^{-1}$
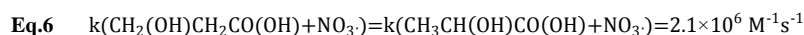
(De Semainville et al., 2007)

3.4.3 Branching ratios

The branching ratios for NO$_3^\bullet$ oxidation are not available in the literature. As a first approach, we use branching ratios for the NO$_3^\bullet$ reactions that are identical to those estimated for HO$^\bullet$ reactions because NO$_3^\bullet$ H-abstraction proceeds following the same elementary mechanism as HO$^\bullet$ H-abstraction. NO$_3^\bullet$ radicals should be more sensitive to steric hindrance than HO$^\bullet$ radicals. However, without experimental evidence supporting this assumption, in our mechanism, NO$_3^\bullet$ radicals are unable to

react *via* electron transfer and to abstract hydrogen atoms from -OH moieties. In these cases, electron transfer and -OH hydrogen abstraction are not included in the list of available $NO_3^•$ reactions, and the remaining pathways are rescaled to 100%. Therefore, for these types of reactions, the branching ratios for $NO_3^•$ oxidation may differ from those for oxidation by $HO^•$

3.5 Reaction with other oxidants

Reactions rates with radicals other than $HO^•$ or $NO_3^•$ are available in the literature (Herrmann et al., 2015; Zellner et al., 1995). They mainly concern reactions of C_{1-2} species with $Cl_2^{•-}$, $CO_3^{•-}$, FeO^{2+} and $SO_4^{•-}$. These reactions are included in the mechanism, and the branching ratios are based on the $HO^•$ reaction branching ratios. However, reactions with these radicals are not included when information in the literature is unavailable, which would require further extension of the CLEPS mechanism when applied to polluted (relatively rich in $SO_4^{•-}$ radicals) or marine (relatively rich in $Cl_2^{•-}$ and other halogenated radicals) environments.

Since our mechanism is developed for low-NO_x conditions, the reactivity of selected oxygenated organic species with H_2O_2 and O_3, which was recently studied by Schöne and Herrmann (2014), is included in the mechanism (see reactions R586 and R590 in the mechanism tables). Although these reactions rates are in the range of 10^{-1} to 10^1 M^{-1} s^{-1}, their impact is non-negligible under specific conditions, especially under low-NO_x conditions. Furthermore, reactions of C_{1-2} hydroperoxide compounds in Fenton-like reactions with Fe^{2+} have been studied by Chevallier et al. (2004) and are included in the mechanism (see reactions R238 and R330 in the mechanism tables).

3.6 Photolysis

Most of the species considered in the mechanism are oxygenated and are likely to bear chromophore functional groups. To calculate the photolysis reaction rate, the polychromatic absorption cross-sections and quantum yields must be known. Again, the literature data concerning these subjects are scarce. Photolysis data are available for a few chromophore species: H_2O_2 (Graedel and Weschler, 1981; Zellner et al., 1990), carboxylate-iron(III) complexes (Faust and Zepp, 1993; Long et al., 2013; Weller et al., 2013a, 2013b), and pyruvic acid (Reed Harris et al., 2014). Absorption cross-section and quantum yield data (preferably wavelength-dependent) are required to calculate photolysis frequencies. Pyruvic acid photolysis is not currently calculated in the model because only the photolysis frequencies are available in the literature.

Because the hydroperoxide (-OOH) moiety is expected to be photosensitive, we include photolysis reactions for species bearing this organic function, using the cross-sections and quantum yields measured for H_2O_2 (as in Leriche et al., 2003). For further improvement, photolysis reactions will be extended to other compounds when experimental data are available to determine which aqueous phase oxygenated compounds are photosensitive.

4. Organic radicals

4.1 Alkyl radical O_2 addition

In dilute aqueous solution, alkyl radicals react with dissolved O_2 to form peroxyl radicals:

R.7 $R·+O_2→R(OO·)$
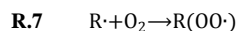
Recent studies suggest that under high organic radical concentrations, this addition competes with the self- or cross-reactions of alkyl radicals, yielding high molecular weight molecules, such as oligomers (see Ervens et al., 2015; Griffith et al., 2013; Lim et al., 2013; Renard et al., 2015). This competition can favour oligomerization if O_2 is not readily available in the aqueous phase. In our mechanism, which is characterised by dilute conditions, dissolved oxygen is assumed to be always available (see Ervens et al., 2015) and alkyl radicals are too dilute to react with themselves. The review by Alfassi (1997)

showed that the kinetics of the great majority of R + O$_2$ reactions are close to the diffusion limit, with rate constants of 2.0–4.0×10^9 M^{-1} s^{-1}, and for non-carbon–centred radicals (such as nitrogen-centred radicals), significantly smaller rate constants are observed (10^7 to 10^8 M^{-1} s^{-1}). Hence, in our mechanism (which does not consider nitrogen-centred radicals), the H-abstraction and O$_2$-addition steps are combined in a single step reaction due to the fast O$_2$-addition reaction rate in the mechanism.

4.2 Tetroxide formation and decomposition

In general, a peroxyl radical reacts with itself or another peroxyl radical to form a tetroxide, which quickly decomposes (von Sonntag and Schuchmann, 1997). These reactions could be introduced to the mechanism by having each peroxyl radical react with every other peroxyl radical. With 363 peroxyl radicals in the mechanism, this would require more than 66,000 reactions to be written to account for theses cross-reactions. As a first approach, we restrict the mechanism to self-reactions. There are available methods to simplify the description of cross-reactions (Madronich and Calvert, 1990). These methods could be adapted for future versions of the mechanism.

The decomposition of tetroxide follows different pathways, depending on the nature of the initial peroxyl radical. Piesiak et al. (1984) proposed a mechanism for the evolution of the tetroxide formed after dimerization of β-hydroxyethylperoxyl radicals. Zegota et al. (1986) studied the self-reaction of the acetonylperoxyl radical and Schuchmann et al. (1985) explored the fate of the acetate peroxyl radical. The results of these studies have been extended in other experimental works for other peroxyl radicals (Liu et al., 2009; Monod et al., 2007; Poulain et al., 2010; Schaefer et al., 2012; Schöne et al., 2014; Stemmler and von Gunten, 2000; Zhang et al., 2010). We therefore implement peroxyl radical self-reactions following the similarity criteria.

For β-peroxycarboxylic acids ($>$C(OO$^\bullet$)C(=O)(OH)) and their conjugated bases, we generalize the experimental results obtained by Schuchmann et al. (1985) for the acetate peroxyl radical (CH$_2$(OO·)C(=O)(O$^-$)). For this radical, the tetroxide is degraded through four pathways (reaction R.8):

R.8 $2\ \text{CH}_2(\text{O}_2\cdot)\text{CO}(\text{O}^-)$

$$\xrightarrow[k_{global}=7.5\times10^7\ \text{M}^{-1}\text{s}^{-1}]{} \text{tetroxide} \rightarrow \begin{cases} \text{CHOCO}(\text{O}^-) + \text{CH}_2(\text{OH})\text{CO}(\text{O}^-) + \text{O}_2 & \text{branching ratio: 30\%} \\ 2\ \text{CHOCO}(\text{O}^-) + \text{H}_2\text{O}_2 & \text{branching ratio: 30\%} \\ 2\ \text{HCHO} + 2\ \text{CO}_2 + \text{H}_2\text{O}_2 + 2\text{OH}^- & \text{branching ratio: 30\%} \\ 2\ \text{CH}_2(\text{O}\cdot)\text{CO}(\text{O}^-) + \text{O}_2 & \text{branching ratio: 10\%} \end{cases}$$
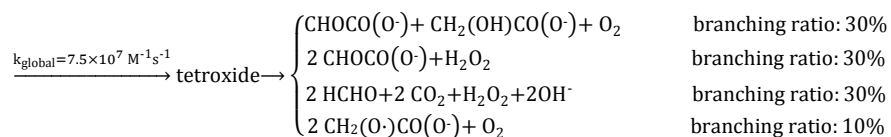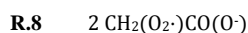
The four pathways retained in this work are the most important identified by Schuchmann et al. (1985). The sum of these pathways contributes to 87% of the tetroxide decomposition, and each individual contribution is scaled to reach 100% overall.

The evolution of β-hydroxyperoxyl radicals ($>$C(OH)C(OO$^\bullet$)$<$) is represented by the experimental results obtained by Piesiak et al. (1984) for the β-hydroxyethylperoxyl radical (CH$_2$(OH)CH$_2$(OO·)) (reaction R.9):

R.9 $2\ \text{CH}_2(\text{OH})\text{CH}_2(\text{OO}\cdot) \xrightarrow{k_{global}=1.0\times10^8\ \text{M}^{-1}\text{s}^{-1}} \text{tetroxide} \rightarrow \begin{cases} \text{CHOCH}_2(\text{OH}) + \text{CH}_2(\text{OH})\text{CH}_2(\text{OH}) + \text{O}_2 & 33\% \\ 2\ \text{CHOCH}_2(\text{OH}) + \text{H}_2\text{O}_2 & 50\% \\ 2\ \text{CH}_2(\text{O}\cdot)\text{CH}_2(\text{OH}) + \text{O}_2 & 17\% \end{cases}$
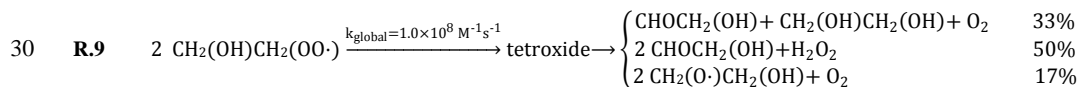
The three pathways are reported to contribute to 90% of the degradation of the tetroxide (Piesiak et al., 1984). The mechanism is restricted to these major pathways, and their individual contributions are scaled to reach 100% overall in our mechanism.

β-oxoperoxyl radicals (-COC(OO$^\bullet$)$<$) are treated based on the studies of the acetonylperoxyl radical by Poulain et al. (2010) and Zegota et al. (1986) (reaction R.10):

R.10 $\quad 2\ CH_3COCH_2(OO\cdot) \xrightarrow{k_{global}=4.0\times10^8\ M^{-1}s^{-1}} tetroxide \rightarrow \begin{cases} CH_3COCH_2(OH) + CH_3COCHO + O_2 & 20\% \\ 2\ CH_3COCHO + H_2O_2 & 45\% \\ 2\ CH_3COCH_2(O\cdot) + O_2 & 35\% \end{cases}$
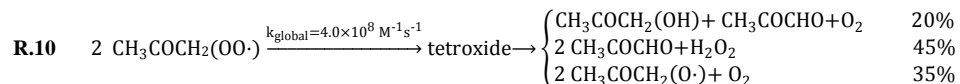
Except for the α-hydroxyperoxyl and acylperoxyl radicals that are discussed in detail in the following subsections, peroxyl radicals that are not included in the above categories are addressed using the estimates from Monod et al. (2007) for the ethylperoxyl radical (reaction R.11):

R.11 $\quad 2\ CH_3CH_2(OO\cdot) \xrightarrow{k_{global}=1.6\times10^8\ M^{-1}s^{-1}} tetroxide \rightarrow \begin{cases} 2\ CH_3CHO + H_2O_2 & 20\% \\ 2\ CH_3CH_2O\cdot + O_2 & 80\% \end{cases}$
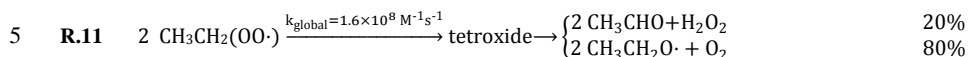
The rate constant was measured by Herrmann et al. (1999). Schuchmann and von Sonntag (1984) estimated that the first pathway (aldehyde pathway) contributes to 20% of the tetroxide decomposition. Studying the ethylperoxyl radical derived from the photooxidation of ethylhydroperoxyde, Monod et al. (2007) found that the second pathway (alkoxyl pathway) is more likely than the aldehyde pathway, in agreement with previous studies (Henon et al., 1997; von Sonntag and Schuchmann, 1997). Therefore, we attributed the remaining degradation of the tetroxide to the alkoxyl pathway.

4.3 α-hydroxyperoxyl HO₂˙/O₂˙⁻ elimination

When a hydroxyl moiety is in the alpha position of the peroxyl function, the peroxyl radical likely undergoes HO₂˙ elimination:

R.12 $\quad >C(OH)(OO\cdot) \rightarrow >C=O + HO_2\cdot$
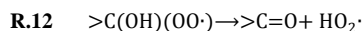
and an O₂˙⁻ elimination following a basic catalysis (Zegota et al., 1986):

R.13 $\quad >C(OH)(OO\cdot) + OH^- \rightarrow >C=O + O_2\cdot^- + H_2O$
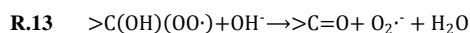
von Sonntag (1987) showed that the HO₂˙ elimination rate constant is dependent on the nature of the substituent attached to the carbon atom. Following this study, we generalized the HO₂˙ elimination rate constants for unknown species using available experimental values. The generalization rules are detailed in **Table 3**.

In the case of α-dihydroxy-peroxyl compounds (-C(OH)(OH)(OO˙)), McElroy and Waygood (1991) showed that HC(OH)(OH)(O₂˙) decays with a rate constant k > 10⁶ s⁻¹. Without additionnal estimates of HO₂˙ elimination, we apply the same elimination rate constant of k = 10⁶ s⁻¹ for all α-dihydroxy-peroxyl compounds. Ilan et al. (1976) and Neta et al. (1990) provided an O₂˙⁻ elimination reaction rate for the 2,α- hydroxypropylperoxyl radical (k(CH₃C(OH)(OO˙)CH₃ + OH⁻) = 5.2×10⁹ M⁻¹ s⁻¹) and the α-hydroxyethylperoxyl radical (k(CH₃CH(OH)(OO˙) + OH⁻) = 4.0×10⁹ M⁻¹ s⁻¹). Given the high concentrations of OH⁻ in water, these reactions are expected to be fast and should not be limiting steps. Therefore, an arbitrary rate constant k = 4.0×10⁹ M⁻¹ s⁻¹, close to the measured reaction rates, is assigned to each elimination reaction.

As shown in **Table 3**, HO₂˙ elimination is a fast process, with an associated lifetime ranging from 1.5×10⁻³ s to 0.1 s. At a concentration of a given peroxyl radical of approximately 10⁻¹⁰ M, tetroxide formation occurs on a timescale of approximately 50 s. Therefore, tetroxide formation and its subsequent decomposition are not considered for α-hydroxyperoxyl radicals, and only direct decomposition is included in the mechanism.

4.4 Acylperoxyl decarboxylation

Acylperoxyl radicals (-CO(OO˙)) are treated like standard peroxyl radicals (see R.11) for which only the alkoxyl formation pathway is considered due to the lack of an H-atom on the peroxyl radical. For the acylperoxyl derived from propionaldehyde, this gives:

R.14 $2\ CH_3CH_2CO(OO\cdot) \xrightarrow{k=1.6\ 10^8\ M^{-1}s^{-1}} \text{tetroxide} \rightarrow 2\ CH_3CH_2CO(O\cdot) + O_2$
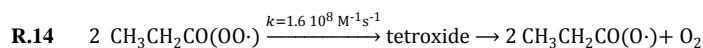
The acylalkoxyl radical undergoes C-C bond scission and yields CO_2, accounting for the expected decarboxylation of the acylperoxyl radical.

4.5 Alkoxyl radicals

Alkoxyl radicals ($RO^\bullet$) are formed after the decomposition of a tetroxide or after the H-abstraction from a –OH functional group. Their reactivity can proceed through two different pathways, 1-2 hydrogen shift (DeCosta and Pincock, 1989):

R.15 $>CH(O\cdot) \rightarrow >C\cdot(OH)$
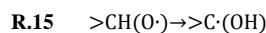
and C-C bond scission (Hilborn and Pincock, 1991):

R.16 $R\text{-}CH(O\cdot)R' \rightarrow >RCH(=O) + R'\cdot$
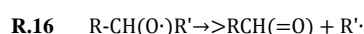
Both pathways are non-limiting steps that are in competition with each other. Schuchmann et al. (1985) studied the fate of acetate peroxyl radicals and showed that the produced alkoxyl radical ($CH_2(O^\bullet)C(=O)(O^-)$) may be degraded following R.15 and R.16. However, they could not determine the relative contribution of both reaction pathways to the degradation of the alkoxyl radical. In our mechanism, bond scission (R.16) is the only possible reaction when a neighbouring carbon atom is oxygenated. The scission leads to the formation of the most stable radicals, *i.e.,* the formation of secondary radicals is favoured over the formation of primary radicals. Alkoxyl radicals evolve through a 1-2 hydrogen shift (R.15) when the neighbouring carbon atoms are not oxygenated.

Because of their very short lifetimes, alkoxyl radicals are not explicitly considered in the mechanism. Instead, electron transfer and fragmentation products are directly included in the global reaction. For example, for the β-hydroxyethylperoxyl radical using the reaction rate and branching ratios from Piesiak et al. (1984) (see R.9):

Pathway 1: $2\ CH_2(OH)CH_2(OO^\bullet) \rightarrow 2\ CHOCH_2(OH) + H_2O_2$	$k = 5.0\ 10^7\ M^{-1}\ s^{-1}$	Piezak et al. (1984)
Pathway 2: $2\ CH_2(OH)CH_2(OO^\bullet) \rightarrow CHOCH_2(OH) + CH_2(OH)CH_2(OH) + O_2$	$k = 3.3\ 10^7\ M^{-1}\ s^{-1}$	Piezak et al. (1984)
Pathway 3: $2\ CH_2(OH)CH_2(OO^\bullet) \rightarrow 2\ CH_2(O^\bullet)CH_2(OH) + O_2$	$k = 1.7\ 10^7\ M^{-1}\ s^{-1}$	Piezak et al. (1984)
$CH_2(O^\bullet)CH_2(OH) \rightarrow C^\bullet H_2(OH) + CH_2O$	Fast	
$C^\bullet H_2(OH) + O_2 \rightarrow CH_2(OH)(OO^\bullet)$	$k = 2.0 \cdot 10^9\ M^{-1}\ s^{-1}$	
$2\ CH_2(OH)CH_2(OO^\bullet) \rightarrow 1.33\ CHOCH_2(OH) + 0.33\ CH_2(OH)CH_2(OH)$	$k = 1.0\ 10^8\ M^{-1}\ s^{-1}$	Piezak et al. (1984)

$+\ 0.34\ CH_2O + 0.34\ CH_2(OH)(OO^\bullet) + 0.50\ H_2O_2 + 0.16\ O_2 - 0.34\ H_2O$

The latter reaction is the overall budget reaction, which is taken into account in the model.

5. Coupling CLEPS with MCM v3.3.1 mass transfer

5.1 Gas phase mechanism

The CLEPS mechanism is coupled to the gas phase Master Chemical Mechanism, MCM v3.3.1 (Jenkin et al., 2015; Saunders et al., 2003) provided at: http://mcm.leeds.ac.uk/MCM. The new version 3.3.1 of MCM includes in particular the treatment of isoprene oxidation products such as epoxydiols, hydroxymethylmethyl-α-lactone (HMML) and methacrylic acid epoxide (MAE).

All gases are dissolved in CLEPS even if they are not further oxidized in the aqueous phase. Conversely, some aqueous species described in CLEPS can be outgassed even if there is no corresponding gas species in MCM. Among the 87 chemical species included in CLEPS, 33 do not have a counterpart in MCM. These are mostly highly oxygenated and highly soluble species. Conversely, 267 gas phase species from MCM have no corresponding aqueous species in CLEPS.

5.2 Estimating mass transfer parameters

Mass transfer is described following the kinetic parameterization from Schwartz (1986). For a given species A:

R.17 $\begin{cases} A_{(g)} \xrightarrow{k_I} A_{(aq)} \\ A_{(aq)} \xrightarrow{k_I/H_A} A_{(g)} \end{cases}$
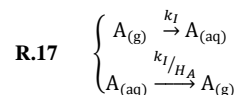
where H_A [M atm^{-1}] is the Henry's law constant for species A and k_I is the pseudo first order rate constant for mass transfer:

R.18 $\quad k_I = Lk_T = L \left(\frac{r^2}{3D_g} + \frac{4r}{3v\alpha} \right)^{-1}$

5 where L [vol. water/vol. air] is the liquid water content of the cloud, r [cm] is the radius of the droplets, D_g [cm^2 s^{-1}] is the gas diffusion coefficient, v [cm s^{-1}] is the mean molecular speed and α [dimensionless] is the mass accommodation coefficient. The parameters H_A, D_g, v, and α are documented for each soluble species in order to fully describe mass transfer. Estimates of unknown parameters are obtained following the approach of Mouchel-Vallon et al. (2013). The Henry's law coefficients are provided by the GROMHE SAR (Raventos Duran et al., 2010). When unavailable, their temperature

10 dependencies (enthalpy of dissolution) are set to 50 kJ mol^{-1}. D_g is calculated by scaling from a reference compound ($\frac{D_{g,A}}{D_{g,H_2O}} = \sqrt{\frac{M_{H_2O}}{M_A}}$; where $D_{g,H_2O} = 0.214/P$ cm^2 s^{-1}, P [atm] is the atmospheric pressure and M$_A$ is the molar mass [g mol^{-1}]; Ivanov et al., 2007). The mean molecular speed is defined as $\sqrt{\frac{8R'T}{\pi M_A}}$ with R'=8.3145 10^7 g cm^2 s^{-2} K^{-1} mol^{-1}. The accommodation coefficients are set to a default value of $\alpha = 0.05$ when no data are available (Davidovits et al., 2006, 2011). We add the temperature dependence of the mass accommodation coefficients based on the parameterization from Nathanson

15 et al. (1996):

R.19 $\quad \frac{\alpha}{1-\alpha} = e^{-\frac{\Delta G_{obs}}{RT}}$

$\Delta G_{obs} = \Delta H_{obs} - T\Delta S_{obs}$ [J mol^{-1}] is interpreted as a the free energy, where ΔH_{obs} [J mol^{-1}] and ΔS_{obs} [J mol^{-1} K^{-1}] are thermodynamic solvation parameters (free enthalpy and entropy) derived by Nathanson et al. (1996) from experimental works on the heterogeneous uptake coefficients performed at different temperatures. When ΔH_{obs} and ΔS_{obs} are

20 experimentally available, they are used to estimate the temperature-dependent α, and in other cases, if the value of α is available in the literature, it is used without the temperature dependency.

5.3 Model description

The mechanism resulting from the coupling of CLEPS with MCM v3.3.1 is integrated in a model based on the Dynamically Simple Model for Atmospheric Chemical Complexity (DSMACC; Emmerson and Evans, 2009) using the Kinetic

25 PreProcessor (KPP: see Damian et al., 2002), which has been modified to account for an aqueous phase, as described in the following. The changes are summarized in blue on **Figure 2**.

Aqueous phase reactions are implemented as a new reaction type. Rate constants in units of M^{-n} s^{-1} are converted to molec^{-n} cm^{-3n} s^{-1}, depending on the constrained liquid water content. Aqueous phase equilibria are decomposed as forward and backward reactions. This alternative to the total species approach used in other models (Leriche et al., 2000) has the

30 drawback of making the ODE (Ordinary Differential Equations) system stiffer. However, in our simulation, the model handles the stiffness without noticeable numerical issues. Moreover, this approach has the advantage of allowing the explicit treatment of cross-equilibria. The pH therefore evolves dynamically as H$^+$ is explicitly produced and consumed in the equilibrium reactions.

Mass transfer is also implemented as a new reaction type. The reaction rates are calculated following Schwartz (1986) and depend on the estimated Henry's law constants, gas diffusion coefficients, mean molecular speeds and accommodation coefficients (see section 5.2).

In DSMACC, TUV 4.5 (Madronich and Flocke, 1997) is used to calculate the photolysis rates in the gas phase (Emmerson and Evans, 2009). The TUV version included in DSMACC was modified to include aqueous phase photolysis reactions (**Figure 2**). To calculate the photolysis coefficients inside the droplets, the clear sky actinic flux values are multiplied by a factor 1.6 (Ruggaber et al., 1997), and the cross-sections and quantum yields are provided from available experimental data (Deguillaume et al., 2004; Long et al., 2013).

Differential equations are solved with a Rosenbrock solver which has been shown to be the most reliable numerical method for stiff ODE systems involved in modelling multiphase chemistry (Djouad et al., 2002, 2003).

6. Simulation of a test case

6.1 Initial conditions

The model is run with the initial and environmental conditions adapted from the low-NO_x situation described by McNeill et al. (2012). Information about the emissions, deposition and initial concentrations of chemical species are provided in **Table 4**. The situation corresponds to summertime conditions, with the simulation starting on the 21st of June. The main difference with the situation described in McNeill et al. (2012) is that isoprene is the only emitted primary organic compound. To compensate for the decrease in total emitted organic mass, the isoprene emission is increased from 1.5×10^6 in McNeill et al. (2012) to 7.5×10^6 molec cm^{-3} s^{-1} in our work. Furthermore, deposition is added for the major oxidation products of isoprene to prevent the accumulation of secondary organic species. The temperature is held constant (290K) during the whole simulation. Under these chemical conditions, the gas chemistry simulation is been run for 31 days (see Supplementary Material **SM3**).

At noon on the 31st day of the simulation, a cloud event is simulated with a constant liquid water content of 3×10^{-7} vol. water/vol. air lasting until midnight with a fixed droplet radius of 10 μm. The cloud event is initialized with 1 μM of iron, which is typical concentrations in continental cloud water (Deguillaume et al., 2014), to enable recycling of oxidants by redox cycles involving iron. The initial pH is set to 4 and is free to evolve. The pH quickly reaches 3.2 (see Supplementary Material **SM4**). An additional simulation is performed to consider the aqueous reactivity of dissolved organic species from the gas phase mechanism, and the reactivity of which is not represented in our aqueous phase mechanism. Each of these dissolved organic species reacts with the HO• radicals with a reaction rate of $k = 3.8 \times 10^8$ M^{-1} s^{-1}. This value is taken from the work of Arakaki et al. (2013), which estimated the sink for aqueous HO• by dissolved organic carbon (DOC). This additional sensitivity test (called "with DOC") is performed to improve the estimate of the HO• concentrations in the atmospheric drops. To account for the conversion of radicals, we assume that each of these reactions produces an HO_2• radical in the aqueous phase.

6.2 Gas chemical reactivity

Figures 3a & 3b show the time evolution of the targeted gases during the 31st day of the gas phase simulation (dashed lines). The NO_x and O_3 mixing ratios (**Figure 3a**) are 0.54 ppbv and 87 ppbv, respectively, at noon while the HO· mixing ratio reaches a maximum of 0.12 pptv. The simulated mixing ratio of isoprene (**Figure 3b**) exhibits a 1.5 ppbv peak in the morning and a minimum of 0.9 ppbv in the afternoon. Because the emission of isoprene is constant during the day in the simulation (and is turned off at night), its time evolution is constrained by the daytime evolution of its oxidants HO• and O_3. In this case, the HO• radical is the main oxidants of isoprene ($k_{HO+isoprene} \times C_{HO} \approx 10 \times k_{O3+isoprene} \times C_{O3}$). Therefore, isoprene

exhibits a minimum at noon when HO⁺ reaches its maximum. The oxidation of isoprene leads to the production of secondary organic species. The time evolutions of the most important secondary species are depicted in **Figure 3b**.

6.3 Impact of aqueous phase reactivity

Figures 3a & 3b show the time evolution of targeted gases during the cloud event (full lines) compared to the gas phase
5 scenario (dashed lines). Previous modelling studies have shown that gas phase HO_x chemistry is modified by the aqueous HO_2⁺ chemistry (Jacob, 1986; Monod and Carlier, 1999). Recent experimental results from Whalley et al. (2015) confirmed that uptake and reactivity in clouds can have a significant impact on the HO_2⁺ and HO⁺ concentrations in the gas phase. In the simulation, at the onset of the cloud event, the HO_2⁺ mixing ratio is reduced by 17%, and the HO⁺ mixing ratios increases by 75%. After an initial sharp decrease, the H_2O_2 mixing ratio exhibits a 50% increase after 4 hours compared to the dry
10 situation. The increase of the HO⁺ mixing ratios is caused by the important dissolution of organic matter, leading to reduced HO⁺ sinks in the gas phase. H_2O_2 is a soluble species, which explains the initial dip in its mixing ratio. The aqueous production of H_2O_2 is responsible for its subsequent higher gaseous levels.

Glyoxal, glycolaldehyde, pyruvic acid, glyoxylic acid and glycolic acid are readily soluble species that react in the aqueous phase (Herrmann et al., 2015). Cloud dissolution and oxidation act as significant sinks for these species. For instance, the
15 glyoxal mixing ratios is reduced by 67% at the start of the cloud event, and the glycolaldehyde mixing ratio is significantly reduced until sunset. For all secondary organic species, daytime gas phase oxidation is increased due to the higher HO⁺ mixing ratios. The addition of aqueous dissolution and aqueous reactive sinks for soluble species explains the sharp decrease in the gas phase mixing ratios for glyoxal, glycolaldehyde, pyruvic acid, glyoxylic acid and glycolic acid. However, the aqueous phase is also a source of secondary organic species. For species that are universal intermediates or end products, the
20 aqueous phase production can be outgassed and contribute to maintaining dry conditions mixing ratios (methylglyoxal, formaldehyde) or significantly increase the mixing ratios compared to dry conditions (acetic and formic acids). Aqueous phase production is also be responsible for introducing an infinitesimal amount of oxalic acid ($< 10^{-9}$ ppbv) into the gas phase, as there is no oxalic acid formation pathway in the gas phase. The addition of the missing aqueous oxidation sink for all dissolved species (red lines in **Figures 3a & 3b**) leads to higher concentrations of species for which reactive uptake is an
25 overall sinks (*e.g.,* glyoxal, glycolaldehyde) because the reduced aqueous HO⁺ concentrations (see **Figure 4**) limit the impact of the aqueous sink. In contrast, lower aqueous HO⁺ concentrations reduce the gas phase mixing ratios of species for which the aqueous phase reactivity is an important source (*e.g.,* formic, acetic and glycolic acids).

Figure 4 shows the time evolution of the main organic aqueous species together with the H_xO_y compounds during the cloud event. The dissolved HO⁺ concentration reaches a peak at 8.5×10^{-14} M, which is similar to dissolved the HO⁺ concentrations
30 simulated by Tilgner et al. (2013) for non-permanent clouds in remote conditions and compiled by Arakaki et al. (2013). The oxalic acid concentration is low during the day (approximately 2×10^{-8} M) because it is present in the form of iron-oxalate complexes, which are readily photolysed. Therefore, during the night, the oxalic acid concentration increases significantly to 10^{-7} M.

The sensitivity test including the additional DOC sink shows that the reduced concentration of HO⁺ radicals (from 8.5 to
35 3×10^{-14} M maximum concentration) decreases the sinks of aqueous species from the gas phase (glycolaldehyde, methylglyoxal and 3,4-dihydroxybutanone), leading to higher aqueous phase concentrations. Conversely, the organic species, which are mostly produced in the aqueous phase (formic, pyruvic, glyoxylic, and oxalic acid) have reduced sources when HO⁺ radicals are scavenged by the added DOC. Their concentrations are therefore lower in these conditions. MACR and MVK are also less sensitive to the DOC addition. Their main source in water is their mass transfer after gas phase
40 production. This is consistent with their behaviour in the gas phase during the cloud event and could explain why they are less sensitive to the HO⁺ concentrations.

A detailed budget of aqueous HO• sinks and sources during the cloud period for the simulation with added DOC (see Supplementary Material **SM5**) shows that H_2O_2 is the main source of HO• *via* the Fenton reaction and its photolysis. The most important overall sink of HO• radicals in the aqueous phase is the reaction with the added DOC (64%), which results in a slight decrease in the simulated aqueous HO• concentrations in **Figure 4**. Besides DOC, simulated reactive organics are the

5   most important HO• sinks, with C_2 compounds contributing to 18%, and C_4 compounds contributing to 12% of HO• destruction. C_1 and C_3 together are responsible for 5% of the HO• sink.

Figure 5 depicts the contributions in term of concentrations of the major species in the aqueous phase. The total concentration of organic matter (continuous line) reaches a maximum of 0.76 mM after 12 hours of cloud simulation, which corresponds to approximately 30 mgC L^{-1}. This value is high but on the order of magnitude of the DOC measurements

10   (Deguillaume et al., 2014; Giulianelli et al., 2014; Herckes et al., 2013, 2015; van Pinxteren et al., 2015). However, species whose reactivity is represented in the CLEPS aqueous mechanism (dashed line in **Figure 5**) constitute only 16% of the total concentration of dissolved species. Not all species dissolved from the MCM undergo a reactive sink in the aqueous phase (see list in Supplementary Material **SM6**). The 10 most abundant species in the aqueous phase contribute to 91% of the concentration of reactive species (126 *vs*. 138 μM) and 15% of the dissolved species. Among these 10 species, glyoxal,

15   hydroxybutanedione, glycoladehyde, 3,4-dihydroxybutanone and glyoxylic and glycolic acids are the most important contributors. A detailed time-resolved flux analysis of the sources and sinks of these species shows that their initial concentration increase is the result of their mass transfer from the gas phase. Then, balance between aqueous sources and sinks defines the time evolution of their concentrations. For instance, the glyoxal concentration continues increasing because of the important source of the aqueous oxidation of glycolaldehyde. The main sink of glycolaldehyde through reaction with

20   HO• is strong enough to make its concentration decrease over time. The two most important acids, glycolic and glyoxylic acids, have initial contributions from gas phase mass transfer and are then produced in the aqueous phase from the oxidation of glyoxal and glycolaldehyde. Acetic and formic acids present simulated concentrations that are in the range of *in situ* measurements. Glycolic and glyoxylic acids present high concentrations in comparison to in situ measurements that should indicate that sources or sinks are therefore likely to be misrepresented in our mechanism.

25   The presence of acids in the main contributors to the aqueous phase organic composition shows the potential for cloud reactivity to be a source of acids. The total amount of organic acids in both phases is almost doubled in less than an hour by the aqueous phase sources, from approximately 0.48 ppbv of gaseous organic acids before the cloud event to a total of 0.98 ppbv of organic acids in both phases (see Supplementary Material **SM7**).

Figure 6 depicts the time evolution of the mean O/C ratio and the mean number of carbon atoms (n_C) in the reactive organic

30   compounds present in the aqueous phase (excluding CO_2 and iron-organic complexes) and in the gas phase (excluding CO and CH_4), with and without the cloud event. The O/C ratios and n_C are a measure of the extent to which long-chain organic species are oxidized and can therefore be a proxy for their functionalization. The reactive aqueous phase is composed of species with an average carbon skeleton of approximately 2.7 carbon atoms and an O/C ratio of 1.1 at the end of the simulation. Large molecules with high functionalization are statistically more soluble than smaller molecules (Mouchel-

35   Vallon et al., 2013; Raventos-Duran et al., 2010). Therefore, at the onset of the cloud event, the larger and more oxygenated species are dissolved, explaining the sharp increase in aqueous n_C at the beginning of the cloud event. In the gas phase, the O/C ratio and n_C follow a marked parabolic curve, reaching a maximum O/C = 0.8 at 15 h and a minimum n_C = 2.3 at 14 h. The O/C ratio and n_C then return to the dry-condition levels at sunset. During the day, cloud reactivity is responsible for the increasing O/C ratios and decreasing n_C. A higher O/C ratio indicates that the number of oxygenated functions per carbon

40   atom has increased. A lower n_C means that, on average, the organic species have a shorter carbon skeleton as a result of cloud reactivity. This suggests that our aqueous mechanism simulates an efficient fragmentation and functionalization of organic compounds.

At the beginning of the cloud event, many oxygenated and large compounds are dissolved leading to an increase in the O/C ratio and n_C in the gas phase. Then, the reactivity in the aqueous phase generates smaller and more oxygenated species that desorb back to the gas phase, and the increase in the O/C ratio is stronger than under clear sky conditions. The observed effects of aqueous reactivity are confirmed by the addition of DOC, which leads to a slower increase in the O/C ratio and a

5   slower decrease in n_C in both phases because lower HO$^\bullet$ radicals concentrations result in a weaker oxidation capacity of the aqueous phase.

7. Conclusions

In this paper we described a new protocol with an explicit chemical scheme for aqueous phase oxidation. This protocol proposes an up-to-date method to describe the dissolution of soluble VOCs, their hydration and/or acid dissociation

10   equilibria (as well as iron-oxalate complexation), their reactivity by direct photolysis and their reactivity with HO$^\bullet$ or NO$_3^\bullet$ radicals. It was developed for dilute conditions and low-NO$_x$ conditions and can be generalized to other, more polluted environments by introducing for example the multiphase reactivity of organonitrates. In this version, the mechanism includes alkanes, alcohols, carbonyls, carboxylic acids and hydroperoxides compounds. The fate of the newly formed organic radicals is also addressed in detail. The protocol is applied to secondary organic species formed in the aqueous phase. Finally, it is

15   formulated in such a way that it could be implemented in automated chemical scheme generation tools, such as GECKO-A (Aumont et al., 2012; La et al., 2016; Mouchel-Vallon et al., 2013).

Under the simulated cloudy conditions, aqueous phase reactivity is shown to impact on the O/C ratio and the size of the secondary organic species, affecting the fragmentation and the functionalization processes resulting from atmospheric oxidation. Furthermore, the addition of a sink for dissolved organic matter shows that this impact on fragmentation and

20   functionalization is sensitive to the aqueous phase oxidative capacity.

As long as the mechanism is used to simulate organic chemistry under dilute conditions, such as in cloud droplets, the hypotheses it is built on remains valid. However, modifications should be performed before applying the model to less dilute atmospheric aqueous phases, such as deliquescent aerosols. First, the non-ideality of such aqueous solutions should be taken into account. Second, H-abstraction and O$_2$-addition should be divided into two distinct steps, and accretion reactions should

25   be considered (Renard et al., 2013). However, the first objective of this work is to thoroughly describe oxidation processes. Accretion processes will be accounted for in future versions of the mechanism. In our simulation, high molecular weight compound precursors, such as glyoxal, glycolaldehyde, and long-chain highly oxygenated species, were dissolved and preferentially formed in the aqueous phase. Models considering radical-initiated oligomer formation are not currently available, except in a few focused cases (Ervens et al., 2015; Woo and Mc Neil 2015). Recent modelling studies

30   implemented newly identified accretion processes to evaluate their potential impacts on SOA formation. However, equivalent accurate knowledge of aqueous oxidation is required since oxidation processes may control the organic radical availability to form accretion products.

Our generated explicit mechanism is based on the Kinetic PreProcessor (KPP) which was built for implementation in chemistry transport 3D models, such as WRF-Chem (Grell et al., 2005) and GEOS-Chem (Eller et al., 2009). The CLEPS

35   mechanism requires some reduction to be coupled with 3D transport models in a similar way to what exists for gas phase chemistry (Emmerson and Evans, 2009; Szopa et al., 2005; Watson et al., 2008) and aqueous phase oxidation (Deguillaume et al., 2009).

This protocol is a powerful tool to explore and propose new reaction mechanisms as a basis to understand experimental studies of scarcely investigated compounds (succinic acid, tartronic acid). The mechanisms generated by our protocol can be

40   used for different purposes in the study of atmospheric aqueous phase processes. They can be evaluated and adapted to laboratory experiments involving a small number of precursors that react only in the aqueous phase. The mechanisms are

more likely to be useful for larger-scale experiments involving longer timescales and two phases (gas + water) in environmental cloud chambers (Brégonzio-Rozier et al., 2016). They are also of interest for the modelling studies of field campaigns such as HCCT (Whalley et al., 2015) or SOAS (Nguyen et al., 2014). The SOA and the cloud chemistry communities are currently interested in studying the respective contributions of oxidation and accretion processes to the

5   transformations of organic matter in the aqueous phase and to the oxidative capacity of clouds. Most recent modelling studies have focused on implementing newly identified accretion processes to evaluate their potential impacts on SOA formation (Ervens et al., 2015; McNeill, 2015; McNeill et al., 2012; Woo and McNeill, 2015). In this work, guidelines are developed to update oxidation mechanisms that will be compared in the future to descriptions of the formation of accretion products, such as oligomers, organonitrates and organosulphates.

10   **Code availability**

The mechanism used in this paper is available in KPP format upon request to l.deguillaume@opgc.univ-bpclermont.fr. Any suggestions and corrections to the mechanism (*e.g.*, new experimental rate constant we may have missed, typos) are also welcomed at the same address. The modified version of DSMACC (originally downloaded at https://github.com/barronh/DSMACC) that was used for the simulations is also available upon request to

15   l.deguillaume@opgc.univ-bpclermont.fr.

Acknowledgments

The authors acknowledge the French National Agency for Research (ANR) project CUMULUS ANR-2010-BLAN-617-01 for providing financial support. The authors are very grateful to the Agence Nationale de la Recherche (ANR) for its financial support through the BIOCAP project (ANR-13-BS06-0004). Part of this work was also supported by CEA/CNRS

20   through the contract CEA 12-27-C-DSPG/CAJ – CNRS 77265.

References

Alfassi, Z. B., Ed.: The Chemistry of Free Radicals: Peroxyl Radicals, Wiley, New York., 1997.

Arakaki, T., Anastasio, C., Kuroki, Y., Nakajima, H., Okada, K., Kotani, Y., Handa, D., Azechi, S., Kimura, T., Tsuhako, A. and Miyagi, Y.: A general scavenging rate constant for reaction of hydroxyl radical with organic carbon in atmospheric

25   waters., Environ. Sci. Technol., 47(15), 8196–203, doi:10.1021/es401927b, 2013.

Asmus, K. D., Moeckel, H. and Henglein, A.: Pulse radiolytic study of the site of hydroxyl radical attack on aliphatic alcohols in aqueous solution, J. Phys. Chem., 77(10), 1218–1221, doi:10.1021/j100629a007, 1973.

Aumont, B., Szopa, S. and Madronich, S.: Modelling the evolution of organic carbon during its gas-phase tropospheric oxidation: development of an explicit model based on a self generating approach, Atmos. Chem. Phys., 5, 2497–2517, 2005.

30   Aumont, B., Valorso, R., Mouchel-Vallon, C., Camredon, M., Lee-Taylor, J. and Madronich, S.: Modeling SOA formation from the oxidation of intermediate volatility n-alkanes, Atmos. Chem. Phys., 12(16), 7577–7589, doi:10.5194/acp-12-7577-2012, 2012.

Blando, J. D. and Turpin, B. J.: Secondary organic aerosol formation in cloud and fog droplets: a literature evaluation of plausibility, Atmos. Environ., 34(10), 1623–1632, 2000.

35   Brégonzio-Rozier, L., Giorio, C., Siekmann, F., Pangui, E., Morales, S. B., Temime-Roussel, B., Gratien, A., Michoud, V., Cazaunau, M., DeWitt, H. L., Tapparo, A., Monod, A. and Doussin, J.-F.: Secondary organic aerosol formation from isoprene photooxidation during cloud condensation–evaporation cycles, Atmos. Chem. Phys., 16(3), 1747–1760, doi:10.5194/acp-16-1747-2016, 2016.

Chevallier, E., Jolibois, R. D., Meunier, N., Carlier, P. and Monod, a.: "Fenton-like" reactions of methylhydroperoxide and

ethylhydroperoxide with Fe^{2+} in liquid aerosols under tropospheric conditions, Atmos. Environ., 38(6), 921–933, doi:10.1016/j.atmosenv.2003.10.027, 2004.

Damian, V., Sandu, A., Damian, M., Potra, F. and Carmichael, G. R.: The kinetic preprocessor KPP-a software environment for solving chemical kinetics, Comput. Chem. Eng., 26(11), 1567–1579, 2002.

5   Darer, A. I., Cole-Filipiak, N. C., O'Connor, A. E. and Elrod, M. J.: Formation and stability of atmospherically relevant isoprene-derived organosulfates and organonitrates., Environ. Sci. Technol., 45(5), 1895–902, doi:10.1021/es103797z, 2011.

Davidovits, P., Kolb, C. E., Williams, L. R., Jayne, J. T. and Worsnop, D. R.: Mass Accommodation and Chemical Reactions at Gas−Liquid Interfaces, Chem. Rev, 106(4), 1323–1354, 2006.

Davidovits, P., Kolb, C. E., Williams, L. R., Jayne, J. T. and Worsnop, D. R.: Update 1 of: Mass Accommodation and
10   Chemical Reactions at Gas−Liquid Interfaces, Chem. Rev, 111(4), 2011.

DeCosta, D. P. and Pincock, J. A.: Control of product distribution by Marcus type electron-transfer rates for the radical pair generated in benzylic ester photochemistry, J. Am. Chem. Soc., 111(24), 8948–8950, doi:10.1021/ja00206a045, 1989.

Deguillaume, L., Leriche, M., Monod, A. and Chaumerliac, N.: The role of transition metal ions on HO$_x$ radicals in clouds: a numerical evaluation of its impact on multiphase chemistry, Atmos. Chem. Phys., 4(1), 95–110, doi:10.5194/acp-4-95-2004,
15   2004.

Deguillaume, L., Leriche, M., Desboeufs, K., Mailhot, G., George, C. and Chaumerliac, N.: Transition Metals in Atmospheric Liquid Phases: Sources, Reactivity, and Sensitive Parameters, Chem. Rev., 105(9), 3388–3431, doi:10.1021/cr040649c, 2005.

Deguillaume, L., Tilgner, A., Schrodner, R., Wolke, R., Chaumerliac, N. and Herrmann, H.: Towards an operational aqueous
20   phase chemistry mechanism for regional chemistry-transport models: CAPRAM-RED and its application to the COSMO-MUSCAT model, J. Atmos. Chem., 64(1), 1–35, 2009.

Deguillaume, L., Charbouillot, T., Joly, M., Vaïtilingom, M., Parazols, M., Marinoni, A., Amato, P., Delort, A.-M., Vinatier, V., Flossmann, A., Chaumerliac, N., Pichon, J. M., Houdier, S., Laj, P., Sellegri, K., Colomb, A., Brigante, M. and Mailhot, G.: Classification of clouds sampled at the puy de Dôme (France) based on 10 yr of monitoring of their physicochemical
25   properties, Atmos. Chem. Phys., 14(3), 1485–1506, doi:10.5194/acp-14-1485-2014, 2014.

Djouad, R., Sportisse, B. and Audiffren, N.: Numerical simulation of aqueous-phase atmospheric models: use of a non-autonomous Rosenbrock method, Atmos. Environ., 36(5), 873–879, doi:10.1016/S1352-2310(01)00497-6, 2002.

Djouad, R., Michelangeli, D. V and Gong, W.: Numerical solution for atmospheric multiphase models: Testing the validity of equilibrium assumptions, J. Geophys. Res., 108(D19), doi:10.1029/2002JD002969, 2003.

30   Donahue, N. M., Kroll, J. H., Pandis, S. N. and Robinson, A. L.: A two-dimensional volatility basis set - Part 2: Diagnostics of organic-aerosol evolution, Atmos. Chem. Phys, 12(2), 615–634, 2012.

Doussin, J.-F. and Monod, A.: Structure–activity relationship for the estimation of OH-oxidation rate constants of carbonyl compounds in the aqueous phase, Atmos. Chem. Phys., 13(23), 11625–11641, doi:10.5194/acp-13-11625-2013, 2013.

Eller, P., Singh, K., Sandu, A., Bowman, K., Henze, D. K. and Lee, M.: Implementation and evaluation of an array of
35   chemical solvers in the Global Chemical Transport Model GEOS-Chem, Geosci. Model Dev., 2(2), 89–96, doi:10.5194/gmd-2-89-2009, 2009.

Emmerson, K. M. and Evans, M. J.: Comparison of tropospheric gas-phase chemistry schemes for use within global models, (1990), 1831–1845, doi:10.5194/acpd-8-19957-2008, 2009.

Epstein, S. A. and Nizkorodov, S. A.: A comparison of the chemical sinks of atmospheric organics in the gas and aqueous
40   phase, Atmos. Chem. Phys., 12(17), 8205–8222, doi:10.5194/acp-12-8205-2012, 2012.

Ervens, B.: Modeling the Processing of Aerosol and Trace Gases in Clouds and Fogs, Chem. Rev., 115(10), 4157–4198, doi:10.1021/cr5005887, 2015.

Ervens, B. and Volkamer, R.: Glyoxal processing by aerosol multiphase chemistry: towards a kinetic modeling framework of

secondary organic aerosol formation in aqueous particles, Atmos. Chem. Phys., 10(17), 8219–8244, 2010.

Ervens, B., George, C., Williams, J. E., Buxton, G. V, Salmon, G. A., Bydder, M., Wilkinson, F., Dentener, F., Mirabel, P., Wolke, R. and Herrmann, H.: CAPRAM 2.4 (MODAC mechanism): An extended and condensed tropospheric aqueous phase mechanism and its application, J. Geophys. Res., 108(D14), 2003.

5   Ervens, B., Feingold, G., Frost, G. J. and Kreidenweis, S. M.: A modeling study of aqueous production of dicarboxylic acids: 1. Chemical pathways and speciated organic mass production, J. Geophys. Res., 109(D15), 2004.

Ervens, B., Turpin, B. J. and Weber, R. J.: Secondary organic aerosol formation in cloud droplets and aqueous particles (aqSOA): a review of laboratory, field and model studies, Atmos. Chem. Phys., 11(21), 11069–11102, 2011.

Ervens, B., Renard, P., Tlili, S., Ravier, S., Clément, J.-L. and Monod, A.: Aqueous-phase oligomerization of methyl vinyl
10 ketone through photooxidation – Part 2: Development of the chemical mechanism and atmospheric implications, Atmos. Chem. Phys., 15(16), 9109–9127, doi:10.5194/acp-15-9109-2015, 2015.

Exner, M., Herrmann, H. and Zellner, R.: Rate constants for the reactions of the NO_3 radical with HCOOH/HCOO$^-$ and CH$_3$COOH/CH$_3$COO$^-$ in aqueous solution between 278 and 328 K, J. Atmos. Chem., 18(4), 359–378, doi:10.1007/BF00712451, 1994.

15 Farmer, D. K., Matsunaga, A., Docherty, K. S., Surratt, J. D., Seinfeld, J. H., Ziemann, P. J. and Jimenez, J. L.: Response of an aerosol mass spectrometer to organonitrates and organosulfates and implications for atmospheric chemistry, Proc. Natl. Acad. Sci., 107(15), 6670–6675, doi:10.1073/pnas.0912340107, 2010.

Faust, B. C. and Zepp, R. G.: Photochemistry of aqueous iron(III)-polycarboxylate complexes: roles in the chemistry of atmospheric and surface waters, Environ. Sci. Technol., 27(12), 2517–2522, doi:10.1021/es00048a032, 1993.

20 Gaillard de Sémainville, P., Hoffmann, D., George, C. and Herrmann, H.: Study of nitrate radical (NO_3) reactions with carbonyls and acids in aqueous solution as a function of temperature., Phys. Chem. Chem. Phys., 9(8), 958–68, doi:10.1039/b613956f, 2007.

Gaillard de Sémainville, P., D Anna, B. and George, C.: Aqueous Phase Reactivity of Nitrate Radicals (NO_3) Toward Dicarboxylic Acids, Zeitschrift für Phys. Chemie, 224(7-8), 1247–1260, doi:10.1524/zpch.2010.6150, 2010.

25 Garnes, L. A. and Allen, D. T.: Size Distributions of Organonitrates in Ambient Aerosol Collected in Houston, Texas, Aerosol Sci. Technol., 36(10), 983–992, doi:10.1080/0278682029009218, 2002.

Giulianelli, L., Gilardoni, S., Tarozzi, L., Rinaldi, M., Decesari, S., Carbone, C., Facchini, M. C. and Fuzzi, S.: Fog occurrence and chemical composition in the Po valley over the last twenty years, Atmos. Environ., 98, 394–401, doi:10.1016/j.atmosenv.2014.08.080, 2014.

30 Graedel, T. E. and Weschler, C. J.: Chemistry within aqueous atmospheric aerosols and raindrops, Rev. Geophys., 19(4), 505, doi:10.1029/RG019i004p00505, 1981.

Grell, G. A., Peckham, S. E., Schmitz, R., McKeen, S. A., Frost, G., Skamarock, W. C. and Eder, B.: Fully coupled "online" chemistry within the WRF model, Atmos. Environ., 39(37), 6957–6975, doi:10.1016/j.atmosenv.2005.04.027, 2005.

Griffith, E. C., Carpenter, B. K., Shoemaker, R. K. and Vaida, V.: Photochemistry of aqueous pyruvic acid, Proc. Natl. Acad.
35 Sci., 110(29), 11714–11719, doi:10.1073/pnas.1303206110, 2013.

Heald, C. L., Kroll, J. H., Jimenez, J. L., Docherty, K. S., DeCarlo, P. F., Aiken, a. C., Chen, Q., Martin, S. T., Farmer, D. K. and Artaxo, P.: A simplified description of the evolution of organic aerosol composition in the atmosphere, Geophys. Res. Lett., 37(8), doi:10.1029/2010GL042737, 2010.

Henon, E., Bohr, F., Chakir, A., Brion, J.: Theoretical study of the methyl peroxy self-reaction: the intermediate structure,
40 Chem. Phys. Let., 264, 557–564, 2007.

Herckes, P., Valsaraj, K. T. and Collett, J. L.: A review of observations of organic matter in fogs and clouds: Origin, processing and fate, Atmos. Res., 132-133, 434–449, doi:10.1016/j.atmosres.2013.06.005, 2013.

Herckes, P., Marcotte, A. R., Wang, Y. and Collett, J. L.: Fog composition in the Central Valley of California over three

decades, Atmos. Res., 151, 20–30, doi:10.1016/j.atmosres.2014.01.025, 2015.

Herrmann, H.: Kinetics of aqueous phase reactions relevant for atmospheric chemistry, Chem. Rev., 103(12), 4691–4716, 2003.

Herrmann, H., Reese, A., Ervens, B., Wicktor, F. and Zellner, R.: Laboratory and modelling studies of tropospheric
5   multiphase conversions involving some C1 and C2 peroxyl radicals, Phys. Chem. Earth part B-Hydrology Ocean. Atmos., 24(3), 287–290, 1999.

Herrmann, H., Tilgner, A., Barzaghi, P., Majdik, Z., Gligorovski, S., Poulain, L. and Monod, A.: Towards a more detailed description of tropospheric aqueous phase organic chemistry: CAPRAM 3.0, Atmos. Environ., 39(23-24), 4351–4363, doi:10.1016/j.atmosenv.2005.02.016, 2005.

10   Herrmann, H., Hoffmann, D., Schaefer, T., Bräuer, P. and Tilgner, A.: Tropospheric aqueous-phase free-radical chemistry: radical sources, spectra, reaction kinetics and prediction tools., Chemphyschem, 11(18), 3796–822, doi:10.1002/cphc.201000533, 2010.

Herrmann, H., Schaefer, T., Tilgner, A., Styler, S. a., Weller, C., Teich, M. and Otto, T.: Tropospheric Aqueous-Phase Chemistry: Kinetics, Mechanisms, and Its Coupling to a Changing Gas Phase, Chem. Rev., 115(10), 4259–4334,
15   doi:10.1021/cr500447k, 2015.

Hilborn, J. W. and Pincock, J. A.: Rates of decarboxylation of acyloxy radicals formed in the photocleavage of substituted 1-naphthylmethyl alkanoates, J. Am. Chem. Soc., 113(7), 2683–2686, doi:10.1021/ja00007a049, 1991.

Ilan, Y., Rabani, J. and Henglein, A.: Pulse radiolytic investigations of peroxy radicals produced from 2-propanol and methanol, J. Phys. Chem., 80(14), 1558–1562, doi:10.1021/j100555a008, 1976.

20   Jacob, D. J.: Chemistry of OH in Remote Clouds and Its Role in the Production of Formic Acid and Peroxymonosulfate, J. Geophys. Res., 91(D9), 9807–9826, 1986.

Jenkin, M. E., Saunders, S. M. and Pilling, M. J.: The tropospheric degradation of volatile organic compounds: A protocol for mechanism development, Atmos. Environ., 31(1), 81–104, 1997.

Jenkin, M. E., Young, J. C. and Rickard, A. R.: The MCM v3.3.1 degradation scheme for isoprene, Atmos. Chem. Phys.,
25   15(20), 11433–11459, doi:10.5194/acp-15-11433-2015, 2015.

Kaul, D. S., Gupta, T., Tripathi, S. N., Tare, V. and Collett J L, J.: Secondary Organic Aerosol: A Comparison between Foggy and Nonfoggy Days, Environ. Sci. Technol., 45(17), 7307–7313, 2011.

Kirkland, J. R., Lim, Y. B., Tan, Y., Altieri, K. E., and Turpin, B. J.: . Glyoxal secondary organic aerosol chemistry: Effects of dilute nitrate and ammonium and support for organic radical-radical oligomer formation, Environ. Chem., 10(3), 158-166,
30   2013.

La, Y. S., Camredon, M., Ziemann, P. J., Valorso, R., Matsunaga, A., Lannuque, V., Lee-Taylor, J., Hodzic, A., Madronich, S. and Aumont, B.: Impact of chamber wall loss of gaseous organic compounds on secondary organic aerosol formation: explicit modeling of SOA formation from alkane and alkene oxidation, Atmos. Chem. Phys., 16(3), 1417–1431, doi:10.5194/acp-16-1417-2016, 2016.

35   Lee, a. K. Y., Hayden, K. L., Herckes, P., Leaitch, W. R., Liggio, J., Macdonald, a. M. and Abbatt, J. P. D.: Characterization of aerosol and cloud water at a mountain site during WACS 2010: secondary organic aerosol formation through oxidative cloud processing, Atmos. Chem. Phys., 12(15), 7103–7116, doi:10.5194/acp-12-7103-2012, 2012.

Lee, A. K. Y., Herckes, P., Leaitch, W. R., Macdonald, A. M. and Abbatt, J. P. D.: Aqueous OH oxidation of ambient organic aerosol and cloud water organics: Formation of highly oxidized products, Geophys. Res. Lett., 38(11), L11805,
40   doi:10.1029/2011GL047439, 2011.

Lee, B. H., Mohr, C., Lopez-Hilfiker, F. D., Lutz, A., Hallquist, M., Lee, L., Romer, P., Cohen, R. C., Iyer, S., Kurtén, T., Hu, W., Day, D. A., Campuzano-Jost, P., Jimenez, J. L., Xu, L., Ng, N. L., Guo, H., Weber, R. J., Wild, R. J., Brown, S. S., Koss, A., de Gouw, J., Olson, K., Goldstein, A. H., Seco, R., Kim, S., McAvey, K., Shepson, P. B., Starn, T., Baumann, K.,

Edgerton, E. S., Liu, J., Shilling, J. E., Miller, D. O., Brune, W., Schobesberger, S., D'Ambro, E. L. and Thornton, J. A.: Highly functionalized organic nitrates in the southeast United States: Contribution to secondary organic aerosol and reactive nitrogen budgets, Proc. Natl. Acad. Sci., 113(6), 1516–1521, doi:10.1073/pnas.1508108113, 2016.

Leriche, M., Voisin, D., Chaumerliac, N., Monod, A. and Aumont, B.: A model for tropospheric multiphase chemistry: application to one cloudy event during the CIME experiment, Atmos. Environ., 34(29-30), 5015–5036, doi:10.1016/S1352-2310(00)00329-0, 2000.

Leriche, M., Deguillaume, L. and Chaumerliac, N.: Modeling study of strong acids formation and partitioning in a polluted cloud during wintertime, J. Geophys. Res., 108(D19), doi:10.1029/2002JD002950, 2003.

Leriche, M., Curier, R. L., Deguillaume, L., Caro, D., Sellegri, K. and Chaumerliac, N.: Numerical quantification of sources and phase partitioning of chemical species in cloud: application to wintertime anthropogenic air masses at the Puy de Dôme station, J. Atmos. Chem., 57(3), 281–297, doi:10.1007/s10874-007-9073-y, 2007.

Lide, D. R. and Frederikse, H. P. R.: Handbook of Chemistry and physics, CRC Press., 1995.

Lim, Y. B., Tan, Y., Perri, M. J., Seitzinger, S. P. and Turpin, B. J.: Aqueous chemistry and its role in secondary organic aerosol (SOA) formation, Atmos. Chem. Phys., 10(21), 10521–10539, 2010.

Lim, Y. B., Tan, Y. and Turpin, B. J.: Chemical insights, explicit chemistry, and yields of secondary organic aerosol from OH radical oxidation of methylglyoxal and glyoxal in the aqueous phase, Atmos. Chem. Phys., 13(17), 8651–8667, doi:10.5194/acp-13-8651-2013, 2013.

Liu, Y., El Haddad, I., Scarfogliero, M., Nieto-Gligorovski, L., Temime-Roussel, B., Quivet, E., Marchand, N., Picquet-Varrault, B. and Monod, A.: In-cloud processes of methacrolein under simulated conditions - Part 1: Aqueous phase photooxidation, Atmos. Chem. Phys., 9(14), 5093–5105, 2009.

Liu, Y., Siekmann, F., Renard, P., El Zein, A., Salque, G., El Haddad, I., Temime-Roussel, B., Voisin, D., Thissen, R. and Monod, A.: Oligomer and SOA formation through aqueous phase photooxidation of methacrolein and methyl vinyl ketone, Atmos. Environ., 49, 123–129, doi:10.1016/j.atmosenv.2011.12.012, 2012.

Long, Y., Charbouillot, T., Brigante, M., Mailhot, G., Delort, A.-M., Chaumerliac, N. and Deguillaume, L.: Evaluation of modeled cloud chemistry mechanism against laboratory irradiation experiments: The HxOy/iron/carboxylic acid chemical system, Atmos. Environ., 77, 686–695, doi:10.1016/j.atmosenv.2013.05.037, 2013.

Madronich, S. and Calvert, J. G.: Permutation reactions of organic peroxy radicals in the troposphere, J. Geophys. Res., 95(D5), 5697, doi:10.1029/JD095iD05p05697, 1990.

Madronich, S. and Flocke, S. J.: Theoretical estimation of biologically effective UV radiation at the Earth's surface, in Solar Ultraviolet Radiation - Modelling, Measurement and Effects, edited by C. Zerefos, pp. 23–48, Springer-Verlag, Berlin., 1997.

McElroy, W. J. and Waygood, S. J.: Oxidation of formaldehyde by the hydroxyl radical in aqueous solution, J. Chem. Soc. Faraday Trans., 87(10), 1513, doi:10.1039/ft9918701513, 1991.

McNeill, V. F.: Aqueous Organic Chemistry in the Atmosphere: Sources and Chemical Processing of Organic Aerosols, Environ. Sci. Technol., 49(3), 1237–1244, doi:10.1021/es5043707, 2015.

McNeill, V. F., Woo, J. L., Kim, D. D., Schwier, A. N., Wannell, N. J., Sumner, A. J. and Barakat, J. M.: Aqueous-Phase Secondary Organic Aerosol and Organosulfate Formation in Atmospheric Aerosols: A Modeling Study, Environ. Sci. Technol., 46(15), 8075–8081, doi:10.1021/es3002986, 2012.

Minakata, D., Li, K., Westerhoff, P. and Crittenden, J.: Development of a Group Contribution Method To Predict Aqueous Phase Hydroxyl Radical (HO•) Reaction Rate Constants, Environ. Sci. Technol., 43(16), 6220–6227, doi:10.1021/es900956c, 2009.

Monod, A. and Carlier, P.: Impact of clouds on the tropospheric ozone budget: Direct effect of multiphase photochemistry of soluble organic compounds, Atmos. Environ., 33(27), 4431–4446, 1999.

Monod, A. and Doussin, J. F.: Structure-activity relationship for the estimation of OH-oxidation rate constants of aliphatic organic compounds in the aqueous phase: alkanes, alcohols, organic acids and bases, Atmos. Environ., 42(33), 7611–7622, doi:10.1016/j.atmosenv.2008.06.005, 2008.

Monod, A., Poulain, L., Grubert, S., Voisin, D. and Wortham, H.: Kinetics of OH-initiated oxidation of oxygenated organic compounds in the aqueous phase: new rate constants, structure-activity relationships and atmospheric implications, Atmos. Environ., 39(40), 7667–7688, doi:10.1016/j.atmosenv.2005.03.019, 2005.

Monod, A., Chevallier, E., Durand-Jolibois, R., Doussin, J., Picquet-Varrault, B. and Carlier, P.: Photooxidation of methylhydroperoxide and ethylhydroperoxide in the aqueous phase under simulated cloud droplet conditions, Atmos. Environ., 41(11), 2412–2426, doi:10.1016/j.atmosenv.2006.10.006, 2007.

Mouchel-Vallon, C., Bräuer, P., Camredon, M., Valorso, R., Madronich, S., Herrmann, H. and Aumont, B.: Explicit modeling of volatile organic compounds partitioning in the atmospheric aqueous phase, Atmos. Chem. Phys., 13(2), 1023–1037, doi:10.5194/acp-13-1023-2013, 2013.

Nathanson, G. M., Davidovits, P., Worsnop, D. R. and Kolb, C. E.: Dynamics and kinetics at the gas-liquid interface, J. Phys. Chem., 100(31), 13007–13020, 1996.

Nguyen, T. B., Roach, P. J., Laskin, J., Laskin, A. and Nizkorodov, S. a.: Effect of humidity on the composition of isoprene photooxidation secondary organic aerosol, Atmos. Chem. Phys., 11(14), 6931–6944, doi:10.5194/acp-11-6931-2011, 2011.

Nguyen, T. K. V., Petters, M. D., Suda, S. R., Guo, H., Weber, R. J., and Carlton, A. G.: Trends in particle-phase liquid water during the Southern Oxidant and Aerosol Study, Atmos. Chem. Phys., 14, 10911-10930, doi:10.5194/acp-14-10911-2014, 2014.

Paulot, F., Crounse, J. D., Kjaergaard, H. G., Kroll, J. H., Seinfeld, J. H. and Wennberg, P. O.: Isoprene photooxidation: new insights into the production of acids and organic nitrates, Atmos. Chem. Phys., 9(4), 1479–1501, doi:10.5194/acp-9-1479-2009, 2009.

Perrin, D. D., Dempsey, B. and Serjeant, E. P.: pKa Prediction for Organic Acids and Bases, Chapman and Hall., 1981.

Perring, A. E., Pusede, S. E. and Cohen, R. C.: An Observational Perspective on the Atmospheric Impacts of Alkyl and Multifunctional Nitrates on Ozone and Secondary Organic Aerosol, Chem. Rev., 113(8), 5848–5870, doi:10.1021/cr300520x, 2013.

Piesiak, A., Schuchmann, M. N., Zegota, H. and von Sonntag, C.: β-Hydroxyethylperoxyl radicals: a study of the γ-radiolysis and pulse radiolysis of ethylene in oxygenated aqueous solutions, Zeitschrift für Naturforschung., 39b, 1262–1267, 1984.

van Pinxteren, D., Fomba, K. W., Mertes, S., Müller, K., Spindler, G., Schneider, J., Lee, T., Collett, J. and Herrmann, H.: Cloud water composition during HCCT-2010: Scavenging efficiencies, solute concentrations, and droplet size dependence of inorganic ions and dissolved organic carbon, Atmos. Chem. Phys. Discuss., 15(17), 24311–24368, doi:10.5194/acpd-15-24311-2015, 2015.

Poulain, L., Katrib, Y., Isikli, E., Liu, Y., Wortham, H., Mirabel, P., Le Calve, S. and Monod, A.: In-cloud multiphase behaviour of acetone in the troposphere: Gas uptake, Henry's law equilibrium and aqueous phase photooxidation, Chemosphere, 81(3), 312–320, 2010.

Raventos-Duran, T., Camredon, M., Valorso, R., Mouchel-Vallon, C. and Aumont, B.: Structure-activity relationships to estimate the effective Henry's law constants of organics of atmospheric interest, Atmos. Chem. Phys., 10(16), 7643–7654, doi:10.5194/acp-10-7643-2010, 2010.

Reed Harris, A. E., Ervens, B., Shoemaker, R. K., Kroll, J. a, Rapf, R. J., Griffith, E. C., Monod, A. and Vaida, V.: Photochemical Kinetics of Pyruvic Acid in Aqueous Solution., J. Phys. Chem. A, doi:10.1021/jp502186q, 2014.

Renard, P., Siekmann, F., Salque, G., Demelas, C., Coulomb, B., Vassalo, L., Ravier, S., Temime-Roussel, B., Voisin, D. and Monod, A.: Aqueous-phase oligomerization of methyl vinyl ketone through photooxidation - Part 1: Aging processes of

oligomers, Atmos. Chem. Phys., 15(1), 21–35, doi:10.5194/acp-15-21-2015, 2015.

Roberts, J. M., Marchewka, M., Bertman, S. B., Goldan, P., Kuster, W., de Gouw, J., Warneke, C., Williams, E., Lerner, B., Murphy, P., Apel, E. and Fehsenfeld, F. C.: Analysis of the isoprene chemistry observed during the New England Air Quality Study (NEAQS) 2002 intensive experiment, J. Geophys. Res., 111(D23), 1–9, doi:10.1029/2006JD007570, 2006.

5   Rollins, A. W., Browne, E. C., Min, K.-E., Pusede, S. E., Wooldridge, P. J., Gentner, D. R., Goldstein, A. H., Liu, S., Day, D. A., Russell, L. M. and Cohen, R. C.: Evidence for NOx Control over Nighttime SOA Formation, Science (80-.)., 337(6099), 1210–1212, doi:10.1126/science.1221520, 2012.

Ruggaber, A., Dlugi, R., Bott, A., Forkel, R., Herrmann, H. and Jacobi, H.-W.: Modelling of radiation quantities and photolysis frequencies in the aqueous phase in the troposphere, Atmos. Environ., 31(19), 3137–3150, doi:10.1016/S1352-2310(97)00058-7, 1997.

10   Saunders, S. M., Pascoe, S., Johnson, A. P., Pilling, M. J. and Jenkin, M. E.: Development and preliminary test results of an expert system for the automatic generation of tropospheric VOC degradation mechanisms, Atmos. Environ., 37(13), 1723–1735, doi:10.1016/S1352-2310(03)00072-4, 2003.

Schaefer, T., Schindelka, J., Hoffmann, D. and Herrmann, H.: Laboratory kinetic and mechanistic studies on the OH-initiated oxidation of acetone in aqueous solution., J. Phys. Chem. A, 116(24), 6317–26, doi:10.1021/jp2120753, 2012.

15   Schöne, L. and Herrmann, H.: Kinetic measurements of the reactivity of hydrogen peroxide and ozone towards small atmospherically relevant aldehydes, ketones and organic acids in aqueous solutions, Atmos. Chem. Phys., 14(9), 4503–4514, doi:10.5194/acp-14-4503-2014, 2014.

Schöne, L., Schindelka, J., Szeremeta, E., Schaefer, T., Hoffmann, D., Rudzinski, K. J., Szmigielski, R. and Herrmann, H.:
20   Atmospheric aqueous phase radical chemistry of the isoprene oxidation products methacrolein, methyl vinyl ketone, methacrylic acid and acrylic acid--kinetics and product studies., Phys. Chem. Chem. Phys., 16(13), 6257–72, doi:10.1039/c3cp54859g, 2014.

Schuchmann, H.-P. and von Sonntag, C.: Methylperoxyl radicals: a study of the γ-radiolysis of methane in oxygenated aqueous solutions, Zeitschrift für Natürforsch., 39b, 217–221, 1984.

25   Schuchmann, M. N., Zegota, H. and von Sonntag, C.: Acetate peroxyl radicals, $O_2CH_2CO_2^-$: a study on the γ-radiolysis and pulse radiolysis of acetate in oxygenated aqueous solutions, Zeitschrift für Naturforschung. Tl. b, Anorg. Chemie, Org. Chemie, 40(2), 215–221, 1985.

Schuchmann, M. N., Schuchmann, H. P. and Von Sonntag, C.: The pKa value of the (carboxymethyl)peroxyl radical: the Taft σ* constant of the -CH_2O_2 group, J. Phys. Chem., 93(13), 5320–5323, doi:10.1021/j100350a055, 1989.

30   Schwartz, S. E.: Mass-transport considerations pertinent to aqueous phase reactions of gases in liquid-water clouds, NATO ASI Ser., G6, 415471, 1986.

von Sonntag, C.: The chemical basis of radiation biology, Taylor & Francis, London., 1987.

von Sonntag, C. and Schuchmann, H.-P.: Peroxyl Radicals in Aqueous Solutions, in The Chemistry of Free Radicals: Peroxyl Radicals, edited by Z. B. Alfassi, Wiley, New York., 1997.

35   Stemmler, K. and von Gunten, U.: OH radical-initiated oxidation of organic compounds in atmospheric water phases: part 2. Reactions of peroxyl radicals with transition metals, Atmos. Environ., 34(25), 4253–4264, 2000.

Tilgner, A. and Herrmann, H.: Radical-driven carbonyl-to-acid conversion and acid degradation in tropospheric aqueous systems studied by CAPRAM, Atmos. Environ., 44(40), 5415–5422, doi:10.1016/j.atmosenv.2010.07.050, 2010.

Tilgner, A., Bräuer, P., Wolke, R. and Herrmann, H.: Modelling multiphase chemistry in deliquescent aerosols and clouds
40   using CAPRAM3.0i, J. Atmos. Chem., 70(3), 221–256, doi:10.1007/s10874-013-9267-4, 2013.

Watson, L. A., Shallcross, D. E., Utembe, S. R. and Jenkin, M. E.: A common representative intermediates (CRI) mechanism for VOC degradation. Part 2: Gas phase mechanism reduction, Atmos. Environ., 42(August), 7196, doi:doi:10.1016/j.atmosenv.2008.07.034, 2008.

Weller, C., Horn, S. and Herrmann, H.: Effects of Fe(III)-concentration, speciation, excitation-wavelength and light intensity on the quantum yield of iron(III)-oxalato complex photolysis, J. Photochem. Photobiol. A Chem., 255, 41–49, doi:10.1016/j.jphotochem.2013.01.014, 2013a.

Weller, C., Horn, S. and Herrmann, H.: Photolysis of Fe(III) carboxylato complexes: Fe(II) quantum yields and reaction mechanisms, J. Photochem. Photobiol. A Chem., 268, 24–36, doi:10.1016/j.jphotochem.2013.06.022, 2013b.

Whalley, L. K., Stone, D., George, I. J., Mertes, S., Van Pinxteren, D., Tilgner, A., Herrmann, H., Evans, M. J. and Heard, D. E.: The influence of clouds on radical concentrations: observations and modelling studies of HO x during the Hill Cap Cloud Thuringia (HCCT) campaign in 2010, Atmos. Chem. Phys, 15, 3289–3301, doi:10.5194/acp-15-3289-2015, 2015.

Woo, J. L. and McNeill, V. F.: simpleGAMMA v1.0 – a reduced model of secondary organic aerosol formation in the aqueous aerosol phase (aaSOA), Geosci. Model Dev., 8(6), 1821–1829, doi:10.5194/gmd-8-1821-2015, 2015.

Zegota, H., Schuchmann, M. N., Schulz, D. and von Sonntag, C.: Acetonylperoxyl radicals, $CH_3COCH_2O_2$: A study on the γ-radiolysis and pulse radiolysis of acetone in oxygenated aqueous solutions, Zeitschrift für Naturforsch., 41b, 1015–1022, 1986.

Zellner, R., Exner, M. and Herrmann, H.: Absolute OH quantum yields in the laser photolysis of nitrate, nitrite and dissolved H_2O_2 at 308 and 351 nm in the temperature range 278-353 K, J. Atmos. Chem., 10(4), 411–425, doi:10.1007/BF00115783, 1990.

Zellner, R., Herrmann, H., Exner, M., Jacobi, H., Raabe, G. and Reese, A.: Formation and Reactions of Oxidants in the Aqueous Phase, in Heterogeneous and Liquid-Phase Processes, edited by P. Warneck, pp. 146–152, Springer-Verlag, Berlin., 1995.

Zhang, X., Chen, Z. M. and Zhao, Y.: Laboratory simulation for the aqueous OH-oxidation of methyl vinyl ketone and methacrolein: significance to the in-cloud SOA production, Atmos. Chem. Phys., 10(19), 9551–9561, doi:10.5194/acp-10-9551-2010, 2010.

Table 1: Experimental hydration constants for carboxylate species.

Species	K_{hyd}	References
Glyoxylate		
CH(=O)C(=O)(O⁻)	67	Tur'yan (1998)
Monoethyl Oxaloacetate		
CH₃CH₂-O-C(=O)C(=O)CH₂C(=O)(O⁻)	3.125	Kozlowski and Zuman (1987)
Pyruvate		
CH₃C(=O)C(=O)(O⁻)	0.0572	Pocker et al. (1969)
α-ketobutyrate		
CH₃CH₂C(=O)C(=O)(O⁻)	0.08	Cooper and Redfield (1975)
α-ketoisovalerate		
CH₃C(CH₃)C(=O)C(=O)(O⁻)	0.075	Cooper and Redfield (1975)
β-fluoropyruvate		
CH₂(F)C(=O)C(=O)(O⁻)	19	Hurley et al. (1969)

Cooper, A. J. L., and Redfield, A. G.: Proton Magnetic-Resonance Studies of Alpha-Keto Acids, J. Biol. Chem., 250, 527–532, 1975.

Hurley, T. J., Carrell, H.L., Gupta, R. K., Schwartz, J., and Glusker, J.P.: The structure of sodium β-fluoropyruvate: A gem-diol, Arch. Biochem. Biophys., 193, 478–486, 1979.
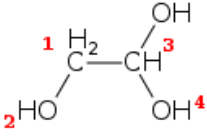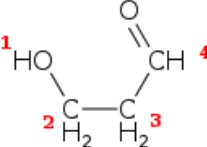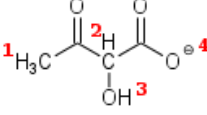
5   Kozlowski, J., and Zuman, P.: Polarographic-reduction of aldehydes and ketones. Effects of acid-base, hydration dehydration and keto enol equilibria on reduction of alpha-ketoglutaric and oxalacetic acid and their esters, J. Electroanal. Chem., 226, 69–102, 1987.

Pocker, Y., Meany, J. E., Nist, B. J., and Zadorojny, C.: Reversible hydration of pyruvic acid, I. Equilibrium studies, J. Phys. Chem., 73, 2879–2882, 1969.

Tur'yan, Y. I.: Kinetics and Equilibrium of the Dehydration-Hydration and Recombination-Dissociation Reactions of Glyoxylic Acid
10   Investigated by Electrochemical Methods, Croat. Chem. Acta, 71, 727–743, 1998.

Table 2: Examples of the reduction scheme applied to estimate HO· reactions branching ratios. k_i values are the partial reaction rate corresponding to the labeled atoms i in the left column.

Molecule	Estimated H-abstraction rates k_i on atom labeled i following Doussin and Monod (2013) [$M^{-1} s^{-1}$]	Contribution to the global reaction rate	Reactivity threshold considered	Retained pathways	Scaled Contribution	Final estimated reaction rates [$M^{-1} s^{-1}$]
Hydrated Glycolaldehyde	$k_1 = 2.9 \times 10^8$	26 %	$C_2 : 90\%$	Yes	28 %	$k_1 = 3.1 \times 10^8$
	$k_2 = 0.9 \times 10^8$	8 %		No	-	-
	$k_3 = 3.4 \times 10^8$	30 %		Yes	33 %	$k_3 = 3.6 \times 10^8$
	$k_4 = 4.0 \times 10^8$	36 %		Yes	39 %	$k_4 = 4.3 \times 10^8$
	$k_{Global} = 1.1 \times 10^9$					$k_{Global} = 1.1 \times 10^9$
3-hydroxypropionaldehyde	$k_1 = 1.5 \times 10^9$	36 %	$C_3 : 75\%$	Yes	38 %	$k_1 = 1.5 \times 10^9$
	$k_2 = 9 \times 10^7$	2 %		No	-	-
	$k_3 = 7 \times 10^7$	2 %		No	-	-
	$k_4 = 2.5 \times 10^9$	60 %		Yes	62 %	$k_4 = 2.6 \times 10^9$
	$k_{Global} = 4.1 \times 10^9$					$k_{Global} = 4.1 \times 10^9$
2-hydroxy, 3-oxobutanoate	$k_1 = 8.1 \times 10^7$	25 %	$C_4 : 75\%$	Yes	31 %	$k_4 = 1.0 \times 10^8$
	$k_2 = 6.1 \times 10^7$	19 %		No	-	-
	$k_3 = 8.5 \times 10^7$	27 %		Yes	33 %	$k_3 = 1.1 \times 10^8$
	$k_4 = 9.2 \times 10^{7\,(*)}$	29 %		Yes	36 %	$k_4 = 1.1 \times 10^8$
	$k_{Global} = 3.2 \times 10^8$					$k_{Global} = 3.2 \times 10^9$

(*) electron transfer reaction

Table 3: Generalization of HO₂· elimination rate constants for unknown species, following von Sonntag (1987).

	von Sonntag (1987) compilation		Generalization
1st Substituent	2nd Substituent	HO₂· elimination rate constant k (s⁻¹)	
H	H	<10	-
H	CH₃	52	Primary peroxyl radicals
H	CH₂(OH)	190	β-hydroxyperoxyl radicals
CH₃	CH₃	665	Secondary peroxyl radicals

Table 4: a) Chemical scenario used for the gas phase simulation of 31 days. b) Aqueous phase initial concentration.

a)

Gas phase species	Initial mixing ratio [ppb]	Emission [molec cm^{-3} s^{-1}]	Deposition [s^{-1}]
SO_2	1	2.91×10^5	1×10^{-5}
NO	-	2.86×10^5	-
NO_2	0.3	-	4×10^{-6}
N_2O_5	-	-	2×10^{-5}
HNO_3	0.3	-	2×10^{-5}
O_3	40	-	4×10^{-6}
H_2O_2	1	-	1×10^{-4}
CH_4	1.7×10^3	-	-
CO_2	3.57×10^5	-	-
CO	1.5×10^2	3.7×10^6	1×10^{-6}
Isoprene	1	7.50×10^{6} [a]	-
Dihydroxybutanone	-	-	5×10^{-5}
MACR	-	-	5×10^{-5}
MVK	-	-	5×10^{-5}
Glyoxal	0.1	-	5×10^{-5}
Methylglyoxal	0.1	-	5×10^{-5}
Glycolaldehyde	-	-	5×10^{-5}
Acetaldehyde	0.1	3.17×10^3	5×10^{-5}
Formaldehyde	0.5	3.03×10^3	5×10^{-5}
Acetone	0.1	8.92×10^3	5×10^{-5}
Pyruvic Acid	-	-	5×10^{-5}
Acetic Acid	1×10^{-3}	3.35×10^3	5×10^{-5}
Formic Acid	-	-	5×10^{-5}
Methanol	2	1.07×10^4	5×10^{-5}
Methylhydroperoxide	0.01	3.35×10^3	5×10^{-6}

[a] = 0 at nighttime, [b] constant

b)

Aqueous phase species	Initial concentrations [μM]
Fe^{2+}	1
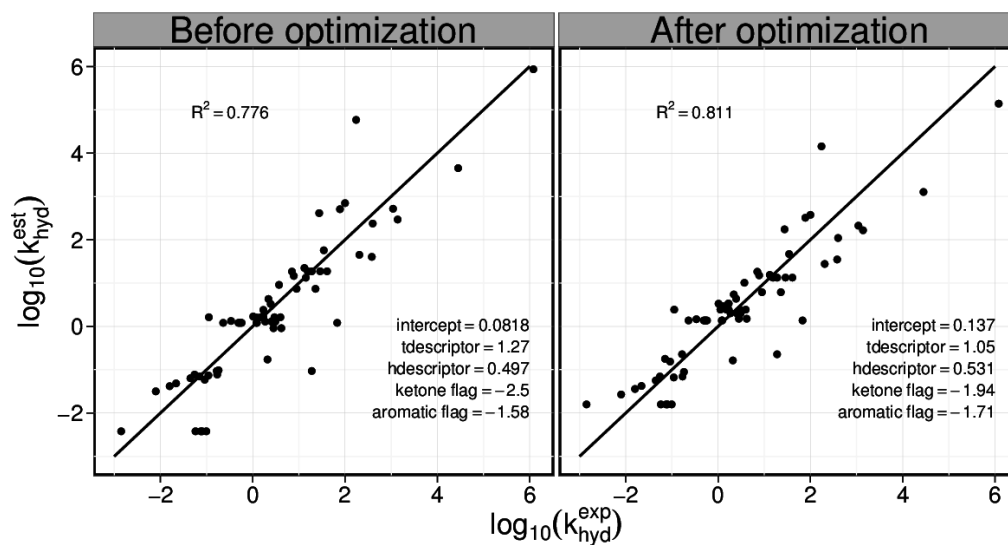
Figure 1: Scatterplots of the estimated $\log(K_{hyd})$ using the SAR from Raventos-Duran et al. (2010) versus the experimental $\log(K_{hyd})$, before (left panel) and after (right panel) the optimization for carboxylates. Values for the optimized descriptors are shown on the bottom right of each panel. The values chosen before the optimization are taken from Raventos-Duran et al. (2010). The line is the $y = x$ line.
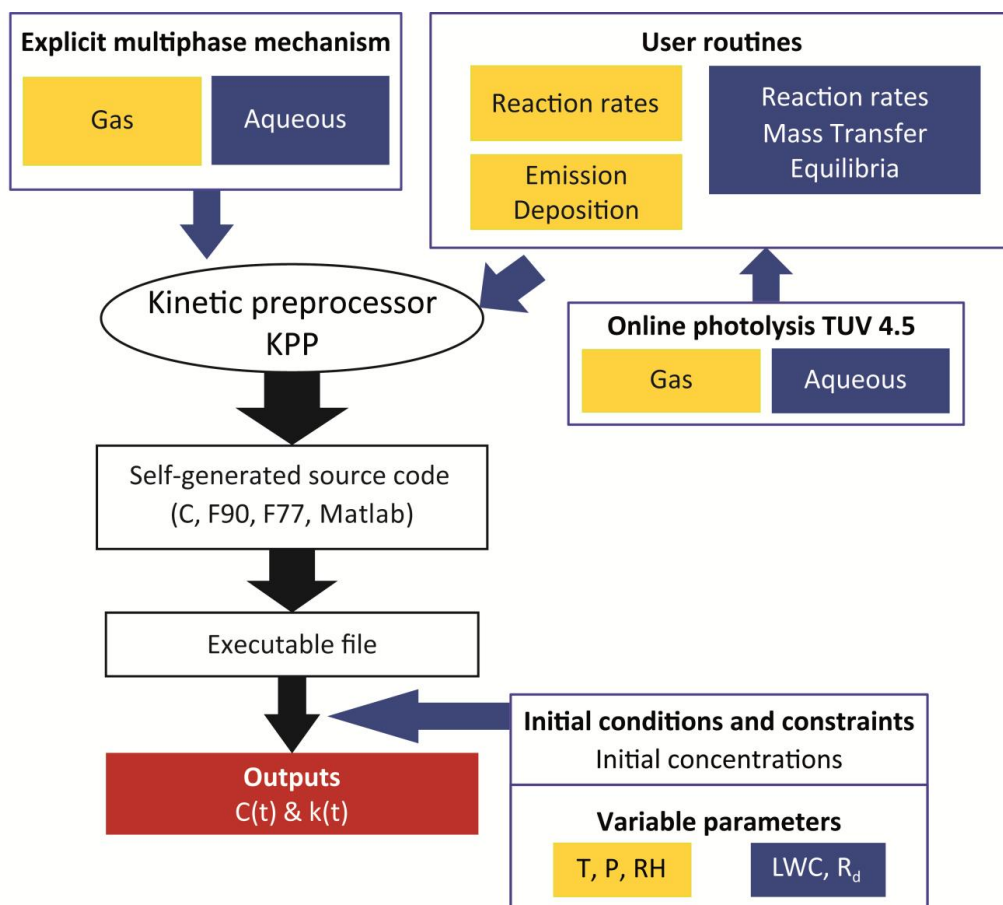
Figure 2: Schematic diagram of the DSMACC version of the Kinetic PreProcessor. The developments relative to aqueous-phase reactivity are shown in blue.

a)

b)
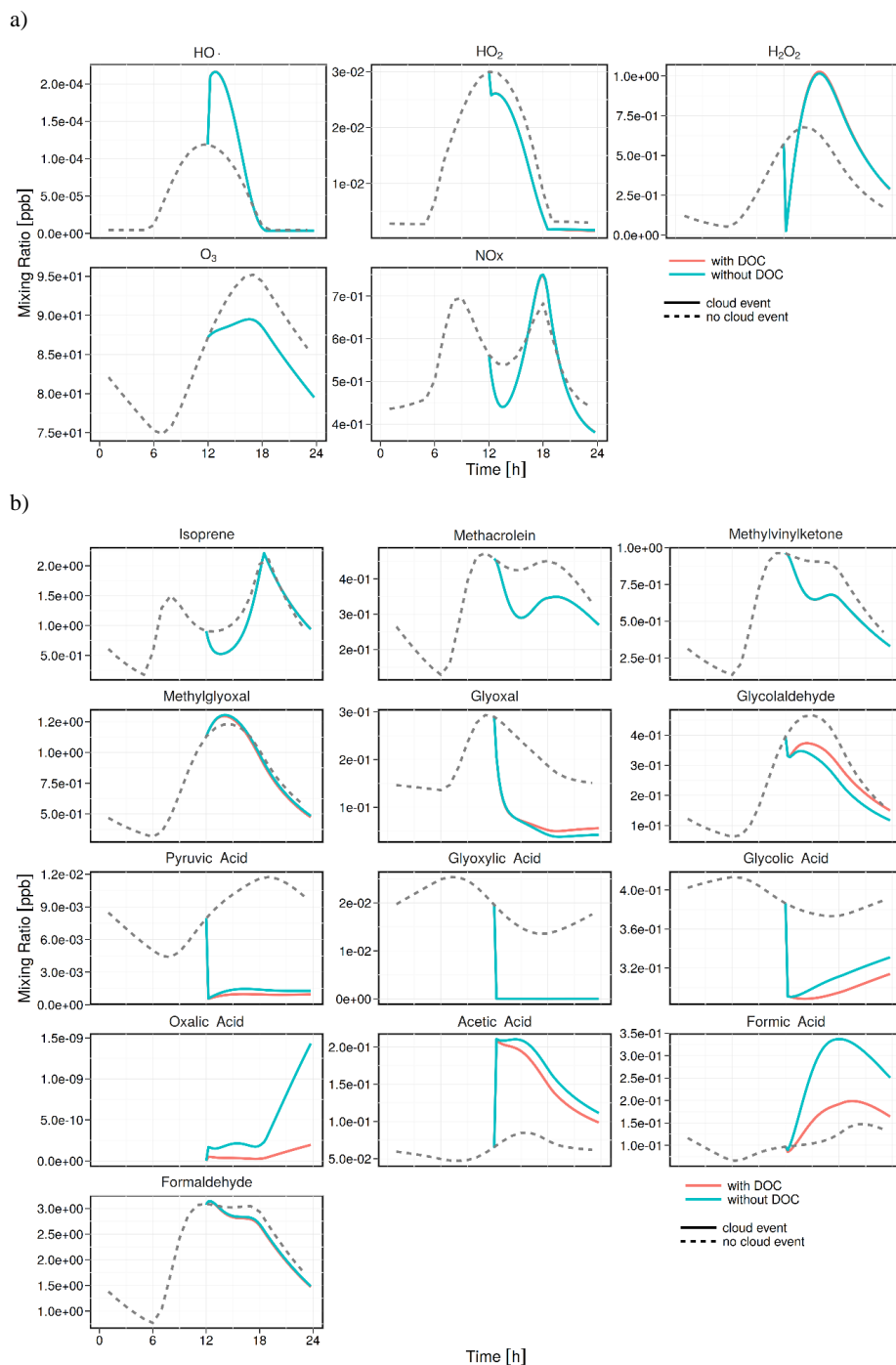
5 **Figures 3a & b: Time evolution of the gas phase mixing ratios without the cloud event (dashed lines) and during the cloud event (continuous line). The cloud event simulations are depicted with (red lines) and without (blue lines) DOC.**
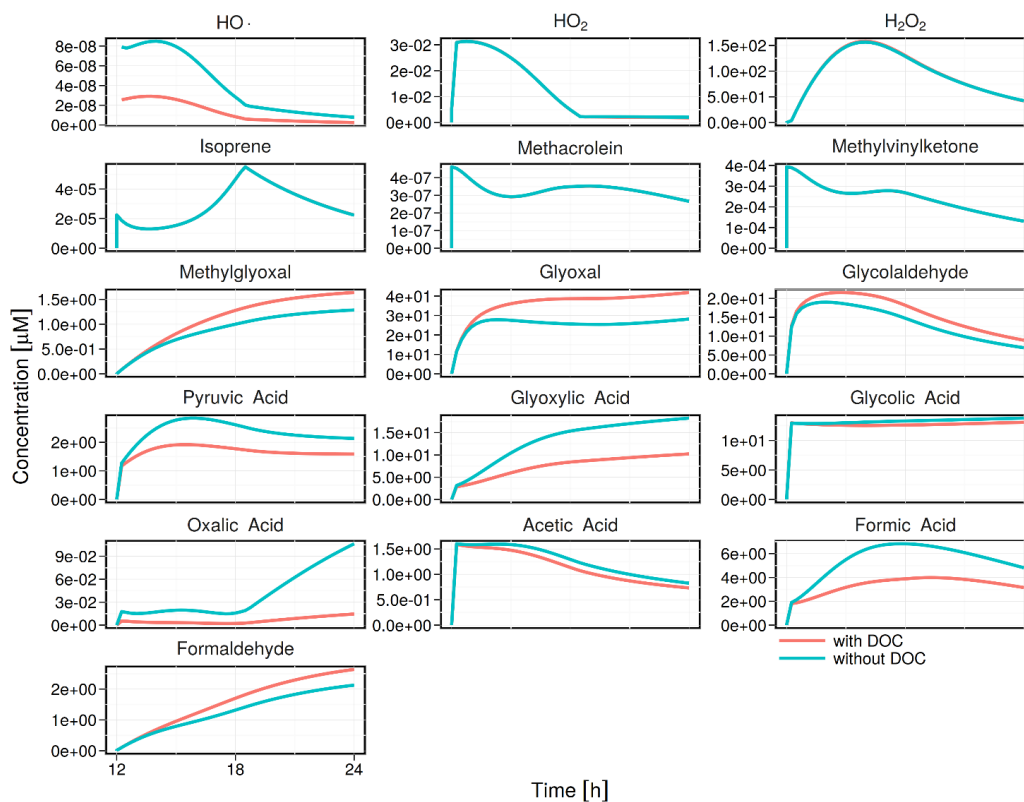
Figure 4: Time evolution of the dissolved species concentrations during the simulated cloud event with (red lines) and without (blue lines) DOC. The vertical scale is in μM; therefore, the HO• radical concentrations are in the 10^{-14} M range.
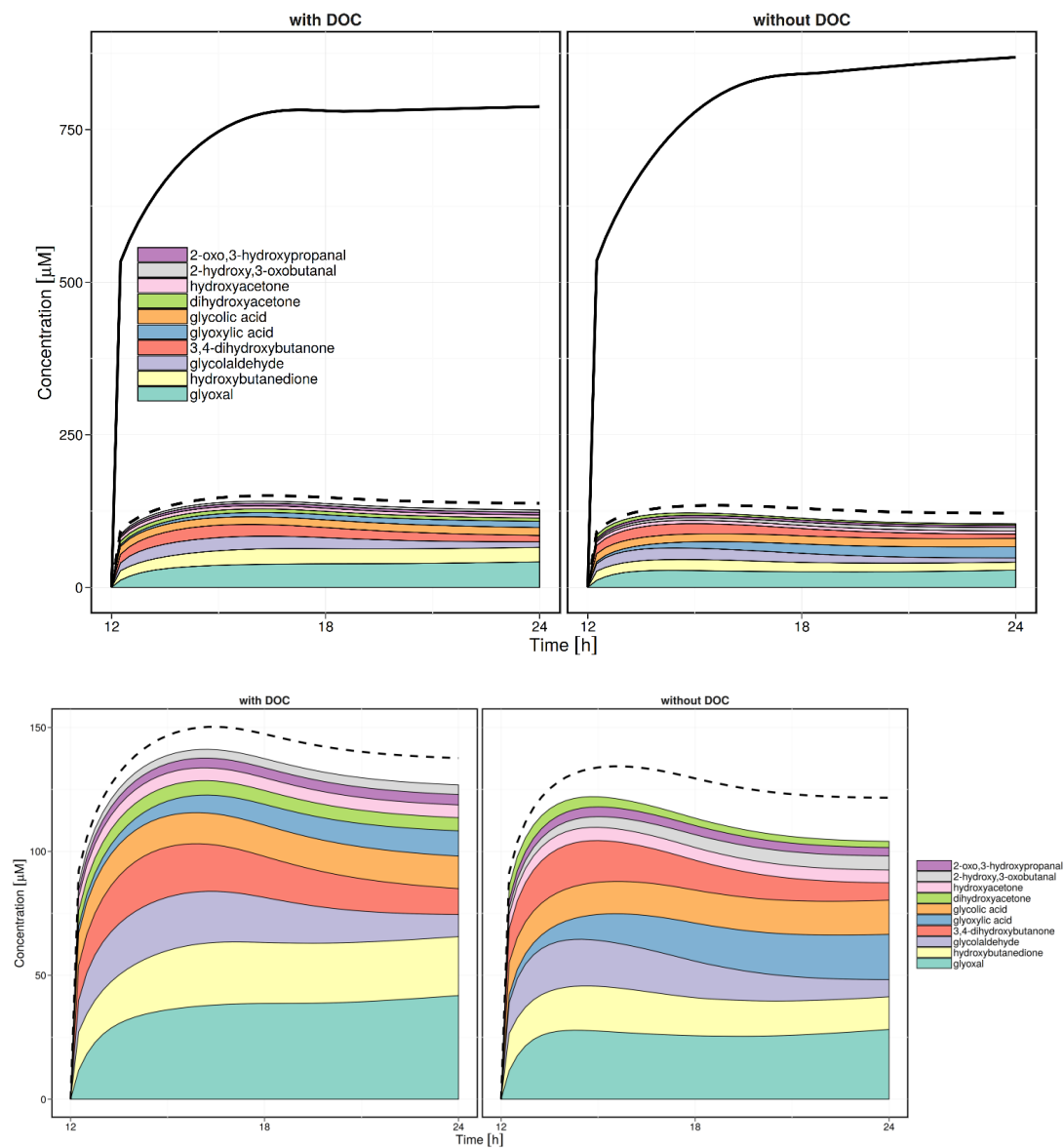
Figure 5: Contribution of the 10 most important species in the aqueous phase (colours). The solid line depicts the total concentration of dissolved organic compounds. The dashed line depicts the total concentration of reactive dissolved species.
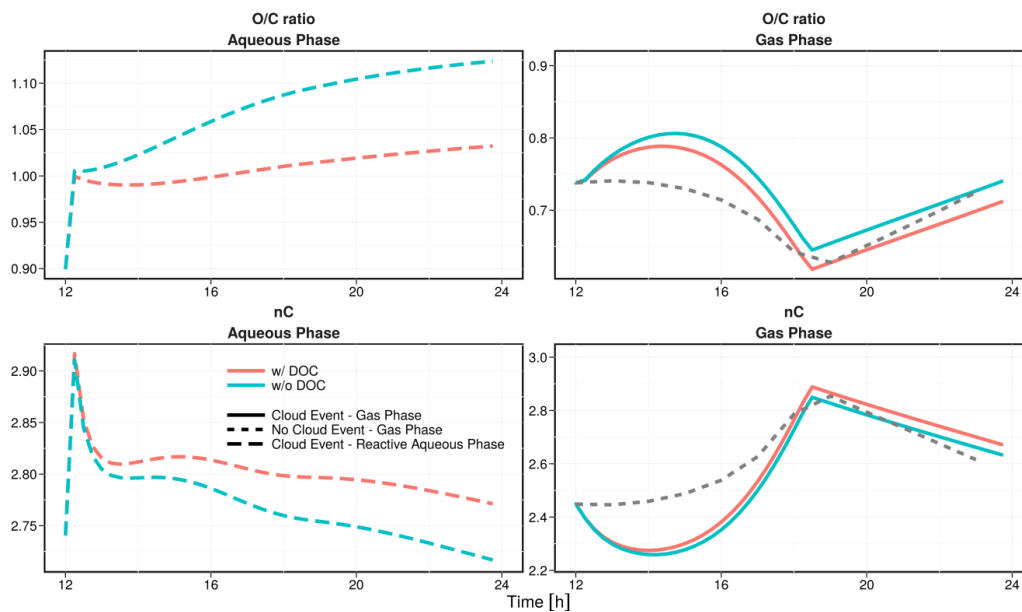
Figure 6: Time evolution of the mean O/C ratio for the reactive species (top; ratios are calculated on a number of atoms basis; CO, CO_2, CH_4, and iron-organic complexes are excluded from the calculation) and the mean number of carbon atoms n_C (bottom) in the aqueous phase (left) and in the gas phase (right) for the gas phase simulation (short dashed lines) and the cloud event simulation (continuous lines). Cloud event simulations are depicted with (red lines) and without (blue lines) DOC.